Article

CRISPR–Cas9 screens reveal regulators of ageing in neural stem cells

https://doi.org/10.1038/s41586-024-07972-2

Received: 23 November 2021

Accepted: 20 August 2024

Published online: 02 October 2024

Open access

Check for updates

Tyson J. Ruetz[1], Angela N. Pogson[1,2,7], Chloe M. Kashiwagi[1,7], Stephanie D. Gagnon[1], Bhek Morton[1], Eric D. Sun[1,3], Jeeyoon Na[1,4], Robin W. Yeo[1], Dena S. Leeman[1], David W. Morgens[1], C. Kimberly Tsui[1], Amy Li[1], Michael C. Bassik[1] & Anne Brunet[1,5,6]✉

Ageing impairs the ability of neural stem cells (NSCs) to transition from quiescence to proliferation in the adult mammalian brain. Functional decline of NSCs results in the decreased production of new neurons and defective regeneration following injury during ageing[1–4]. Several genetic interventions have been found to ameliorate old brain function[5–8], but systematic functional testing of genes in old NSCs—and more generally in old cells—has not been done. Here we develop in vitro and in vivo high-throughput CRISPR–Cas9 screening platforms to systematically uncover gene knockouts that boost NSC activation in old mice. Our genome-wide screens in primary cultures of young and old NSCs uncovered more than 300 gene knockouts that specifically restore the activation of old NSCs. The top gene knockouts are involved in cilium organization and glucose import. We also establish a scalable CRISPR–Cas9 screening platform in vivo, which identified 24 gene knockouts that boost NSC activation and the production of new neurons in old brains. Notably, the knockout of *Slc2a4*, which encodes the GLUT4 glucose transporter, is a top intervention that improves the function of old NSCs. Glucose uptake increases in NSCs during ageing, and transient glucose starvation restores the ability of old NSCs to activate. Thus, an increase in glucose uptake may contribute to the decline in NSC activation with age. Our work provides scalable platforms to systematically identify genetic interventions that boost the function of old NSCs, including in vivo, with important implications for countering regenerative decline during ageing.

The adult mammalian brain contains several NSC regions that give rise to newborn neurons and can repair tissue damaged by stroke or brain injuries[1,4,9–14]. The most active NSC niche is located in the subventricular zone (SVZ) that lines the lateral ventricles of the brain[1,2,4,10,13–18]. NSCs from the SVZ region can generate thousands of newborn neurons each day in a young adult mouse[10]. The SVZ region comprises a pool of quiescent NSCs (qNSCs) that can give rise to activated (proliferating) NSCs (aNSCs), which in turn generate more committed progenitors that migrate out of the niche towards the olfactory bulb, where they differentiate into neurons. The ability of NSCs to activate and form newborn neurons is severely impaired in the ageing brain, and this can contribute to deficits in sensory and cognitive function[1–3,15,19–23].

Identifying genes that affect NSC activation could lead to interventions that counter brain defects during ageing. Several genetic interventions, including signalling pathways and transcriptional regulators, have been shown to improve activation of old NSCs[5–8,24–27]. However, such studies have been limited in their throughput as they focus on one or a few genes at a time. Thus, we are still lacking a systematic understanding of the genes and pathways that functionally affect old NSCs.

More generally, a major challenge in identifying genetic interventions that improve the function of old cells is the establishment of scalable genetic screens in mammals. Ageing occurs at both the cell and organismal levels; therefore, it is important to develop screens in vitro in cells from old organisms and in vivo in old tissues. CRISPR–Cas9 genome-wide screens have been developed for several phenotypes in vitro[28–36], including with stem cell models of Werner and Hutchinson–Gilford progeria syndrome[37]. However, genetic screens for regulators of ageing in normal old cells have not yet been performed. In addition, in vivo genetic screens are challenging in mammals and have currently been limited to development[38–40], young tissues[41–43] or cancer[36,44–47]. Thus, developing CRISPR–Cas9 screening platforms for old mammalian cells and organisms has the potential to identify previously unknown gene manipulations that could restore tissue function in older individuals. In the brain, such screens could help identify strategies to counter regenerative and cognitive decline with ageing.

CRISPR–Cas9 screen to boost old NSCs

To systematically identify genes that boost NSC activation as a function of age, we developed a genetic screening platform to conduct genome-wide CRISPR–Cas9 knockout screens in primary NSC cultures from young and old mice (Fig. 1a; see Fig. 2 for in vivo targeted

[1]Department of Genetics, Stanford University, Stanford, CA, USA. [2]Developmental Biology Graduate Program, Stanford University, Stanford, CA, USA. [3]Biomedical Informatics Graduate Program, Stanford University, Stanford, CA, USA. [4]Stem Cell Biology & Regenerative Medicine Graduate Program, Stanford University, Stanford, CA, USA. [5]Glenn Center for the Biology of Aging, Stanford University, Stanford, CA, USA. [6]Wu Tsai Neurosciences Institute, Stanford University, Stanford, CA, USA. [7]These authors contributed equally: Angela N. Pogson, Chloe M. Kashiwagi. ✉e-mail: abrunet1@stanford.edu

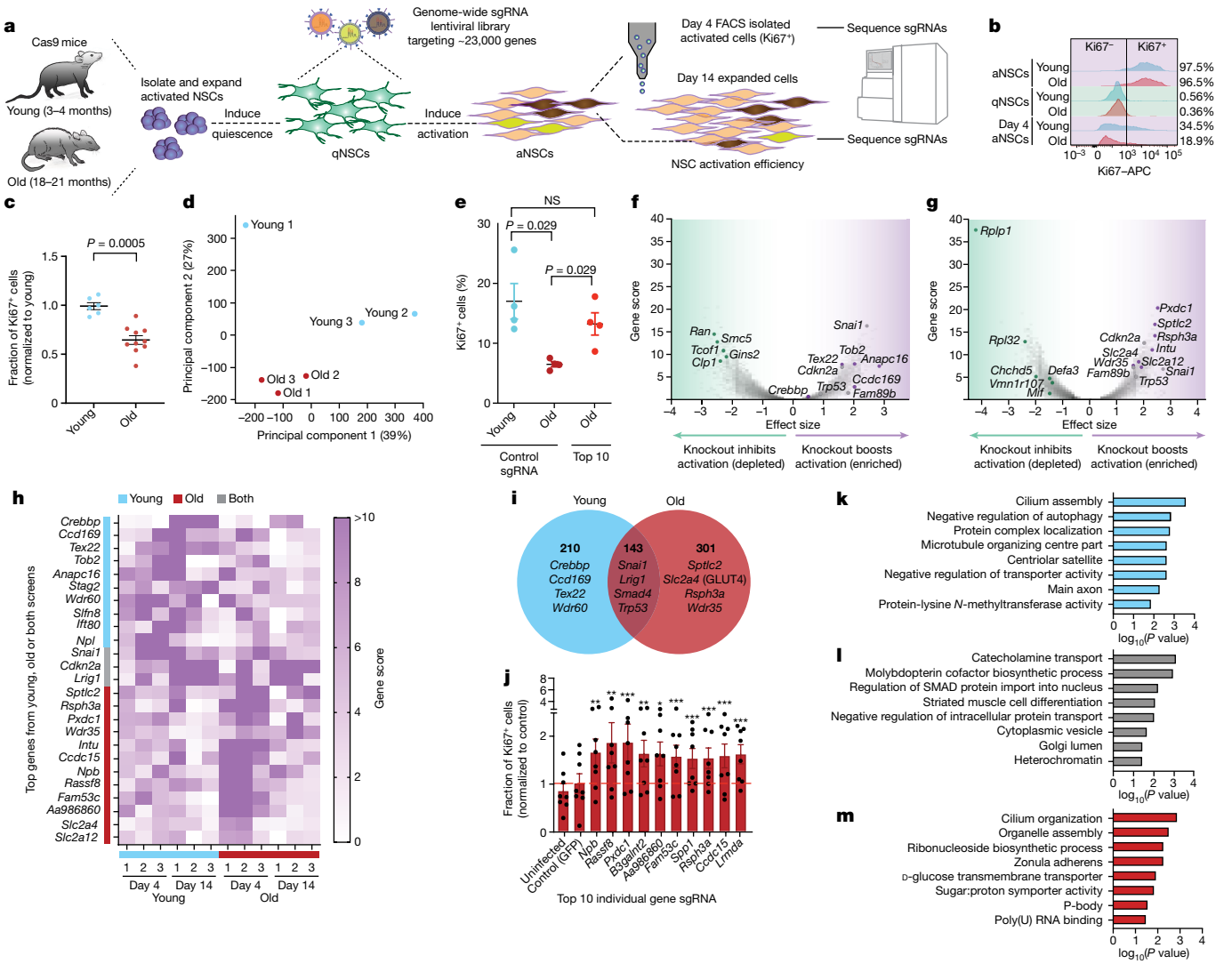

Fig. 1 | A genome-wide screen identifies 300 gene knockouts that boost old NSC activation. a, Screen design. Three independent genome-wide screens used primary NSC cultures, each from six pooled young (3–4 months old) or six pooled old (18–21 months old) Cas9 mice (three males, three females). **b**, Example Ki67 FACS of NSCs from young and old Cas9 mice. **c**, Quantification (FACS) of NSC activation efficiency at day 4. Mean ± s.e.m. of Ki67$^+$ cell percentage (normalized to young) for $n = 6$ (young) and $n = 10$ (old) NSC cultures, each from six pooled Cas9 mice (three males, three females), over three experiments. Each dot represents one NSC culture. Two-tailed Mann–Whitney test. **d**, PCA of gene scores of each screen (day 14). **e**, NSC activation efficiency quantification (FACS). Mean ± s.e.m. of percentage of Ki67$^+$ cells for $n = 4$ (young control), $n = 4$ (old control), $n = 4$ (old top 10) NSC cultures, each from six pooled Cas9 mice (three males, three females), over two experiments. Each dot represents one NSC culture. Control, 100 control sgRNAs; top 10, sgRNAs targeting the top 10 genes from screens 1 and 2 (day 4 or 14, FDR < 0.1). Two tailed Mann–Whitney test. NS, not significant. **f**,**g**, Example results (screen 2) for young (**f**) and old (**g**) NSCs at day 4, showing gene scores as a function of effect size. Each dot represents one gene. Coloured dots indicate top gene knockouts (FDR < 0.1 in at least two out of three screens, day 4 or day 14) that boost (purple) or impede (green) NSC activation in an age-dependent manner or boost activation regardless of age (grey). **h**, Heatmap showing gene scores for top gene knockouts that boost young or old NSC activation. **i**, Venn diagram of gene knockouts that boost young or old NSC activation in at least two out of three screens (FDR < 0.1). **j**, Quantification of old NSC activation efficiency (FACS) (individual validation). Mean ± s.e.m. of percentage of Ki67$^+$ cells (normalized to control) for $n = 8$ NSC cultures (each condition), each from two pooled old Cas9 mice (one male and one female), over two experiments. Each dot represents one NSC culture. Top 10 genes, 5 sgRNAs per gene. Two-tailed Wilcoxon signed rank test. *P* values in source data. **k**–**m**, Selected GO terms associated with genes knockouts that boost young (**k**), young and old (**l**) or old (**m**) NSC activation in at least two out of three screens (FDR < 0.1) using EnrichR. One-sided Fisher's exact test.

screens). Primary NSC cultures can transition between qNSC and aNSC states in culture when exposed to different growth factors[48]. Primary qNSC cultures from old mice exhibit a decreased ability to activate compared with their young counterparts, thereby recapitulating an in vivo ageing phenotype[25]. To establish a screening platform, we aged cohorts of mice that express Cas9 (and eGFP) in all cells, hereafter termed Cas9 mice[49] (Methods). For each independent screen (three in total), we collected NSCs from the SVZ of 6 young (3–4 months old) and 6 old (18–21 months old) Cas9 mice. As expected, primary qNSC cultures from old Cas9 mice displayed an impeded ability to activate compared with young counterparts (about twofold decline based on the proliferation marker Ki67) (Fig. 1b,c).

We performed three independent genome-wide CRISPR–Cas9 screens for genes that affect qNSC activation as a function of age. To this end, we expanded NSCs from young and old Cas9 mice, induced quiescence and then transduced more than 400 million qNSCs with lentiviruses that express a single guide RNA (sgRNA) library targeting around 23,000 protein-coding genes in the genome, with 10 unique sgRNAs per gene, as well as 15,000 control sgRNAs (about 245,000 sgRNAs in total)[29] (Fig. 1a). Five days after sgRNA library transduction,

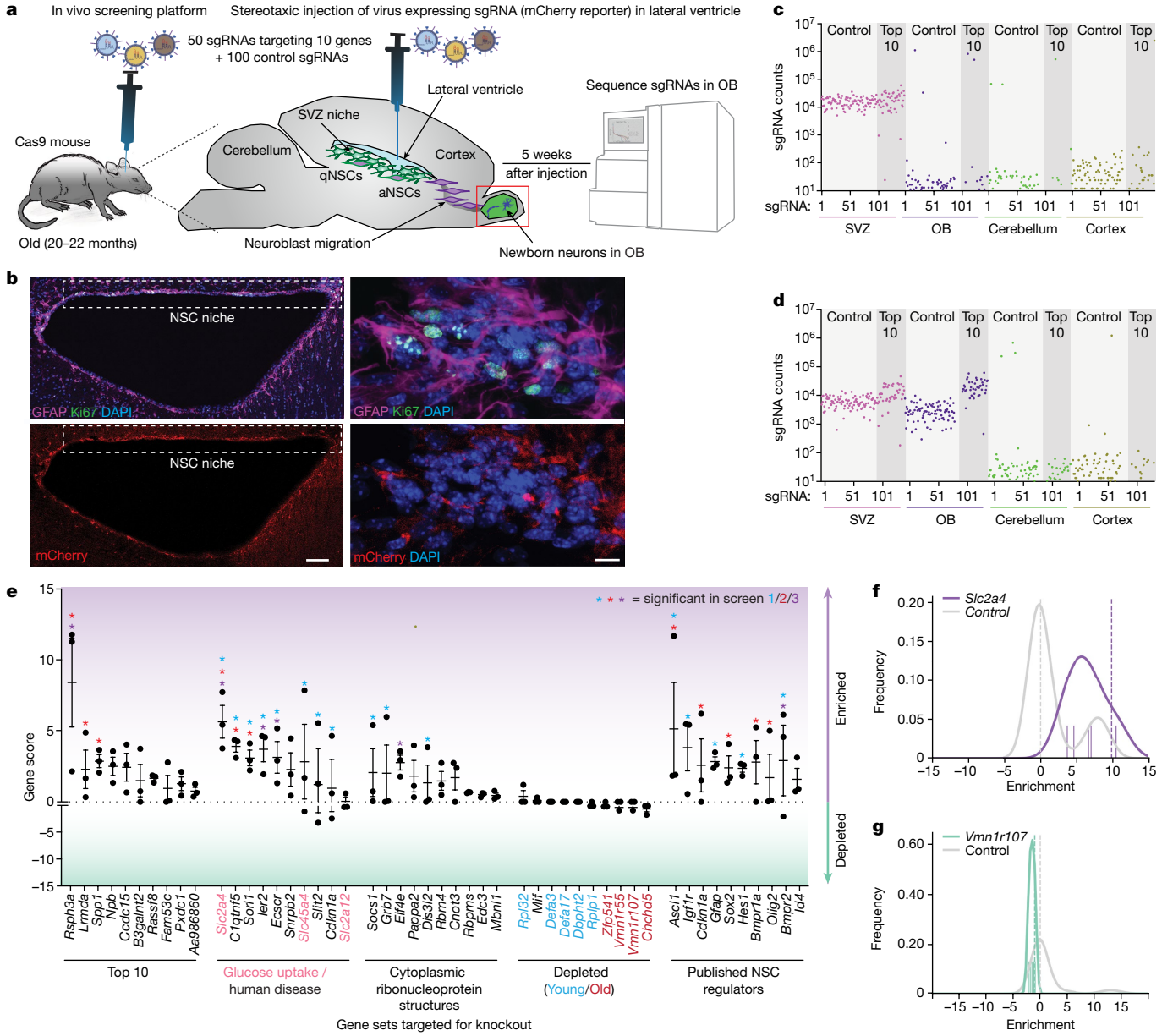

Fig. 2 | In vivo screening platform for rapid testing of gene knockout effects on NSC activation. a, In vivo screen platform in old mice. Old (20–22 months) Cas9 mice were injected with lentivirus expressing sgRNAs into the lateral ventricles (in proximity to the SVZ NSC niche). Five weeks after injection, genomic DNA was collected from the olfactory bulb (OB), and sgRNAs were sequenced to determine enrichment or depletion. **b**, Immunofluorescence images of SVZ niche sections from old (21 months) Cas9 mice, 48 h after injection of lentiviruses expressing mCherry and 100 control sgRNAs. One experiment. mCherry (lentivirus-infected cells, red), GFAP (NSCs and astrocytes, magenta), Ki67 (proliferative cells, green), DAPI (nuclei, blue). Right, high-magnification images. Scale bars, 100 µm (left); 10 µm (right). **c**,**d**, Normalized sgRNA counts of the top 10 gene pool (50 sgRNAs) and control (100 sgRNAs) libraries in various brain regions, 1 day (**c**) or 5 weeks (**d**) after virus injection. Top 10 gene pool, gene knockouts that boosted old NSC activation in in vitro screens 1 and 2. sgRNA counts were normalized to total counts between brain regions to account for sequencing depth variance. **e**, CasTLE gene scores for 50 gene knockouts tested in groups of 10 in old (19–22 months) female Cas9 mice, analysing for enrichment or depletion in the OB. Each sgRNA library of 10 genes was injected into $n = 4$ old Cas9 mice, $n = 1$ mouse for 1 day after injection SVZ sequencing of starting sgRNA pool, and $n = 3$ mice for 5 weeks after injection sequencing of OB sgRNAs. OB sgRNA enrichment computed with CasTLE and comparing with the 24-h SVZ sequenced sample. Mean ± s.e.m. of CasTLE score in $n = 3$ mice. Each dot represents the gene score from one mouse. Asterisks indicate gene hits with a 95% confidence interval that did not contain 0 by CasTLE analysis. Colour indicates screen number. **f**,**g**, Relative enrichment and frequency of each sgRNA targeting *Slc2a4* (purple), *Vmn1r107* (green) or control (grey) sgRNA pool in the OB. Hashed line: CasTLE-computed relative enrichment effect size for sgRNAs of interest relative to control sgRNA pool. Vertical dashed lines indicate relative enrichment of the five sgRNAs targeting *Slc2a4* or *Vmn1r107*.

qNSCs were activated with growth factors and expanded for either 4 or 14 days and processed as independent samples for sequencing (Fig. 1a). The day 4 timepoint was chosen to isolate any cell that was successfully activated by fluorescence-activated cell sorting (FACS) based on the proliferation marker Ki67. The day 14 timepoint enabled the enhanced enrichment of cells with knockouts that maintained self-renewal capabilities over long periods of time and outgrew other cells and therefore did not require FACS isolation. After 4 or 14 days, we generated libraries of sgRNAs from all cells and processed them for high-throughput sequencing. The sgRNA libraries had sufficient coverage of the sgRNA pool for genome-wide screen analysis (Extended Data Fig. 1a–c).

To analyse each screen sample, we assessed sgRNA enrichment or depletion by CasTLE analysis[28], which uses the sequencing read counts of the 10 sgRNAs targeting each gene and compares them with the control sgRNA distributions to compute effect size, gene score, confidence interval and *P* value. The results of each screen correlated with each other (although 'young day 14' was a slight outlier for screen 1) (Extended Data Fig. 1d–f). Principal component analysis (PCA) on CasTLE gene score values mostly separated the three independent screens on the basis of NSC age (Fig. 1d and Extended Data Fig. 1g–i), which highlighted that ageing is a primary contributor to the outcome of the screen. We independently verified that a subscreen of the top 10 gene knockouts that improved old NSC activation in screens 1 and 2 (Supplementary Table 3) could boost, as a pool, old NSC activation to around 70% of young NSC activation levels (Fig. 1e).

We then directly compared young and old NSC screens to identify the gene knockouts that boost NSC activation specifically in young NSCs, specifically in old NSCs or regardless of age (Fig. 1f–i, Extended Data Fig. 1j,k and Supplementary Table 1). Overall, our genome-wide screens identified 654 and 1,386 genes for which knockouts boosted or impeded NSC activation, respectively (false discovery rate (FDR) < 0.1 in 2 or more independent screens; Supplementary Table 1). As expected, gene knockouts that impeded NSC activation overlapped with essential genes (Extended Data Fig. 1l,m). We identified 143 gene knockouts that enhanced both young and old NSC activation, 210 specific to young NSC activation and 301 specific to old NSC activation (Fig. 1i and Supplementary Table 1). We individually validated the top 10 gene knockouts that ameliorated old NSC activation in screens 1 and 2 (Supplementary Table 3). We verified individual knockout efficiency at the genomic level (Extended Data Fig. 1n). Notably, 10 out of these 10 individual gene knockouts indeed boosted old NSC activation as assessed by $Ki67^+$ FACS analysis (Fig. 1j).

Consistent with previous findings, genes implicated in the maintenance of NSC quiescence (for example, *Snai1*, *Smad4* (TGFβ pathway) and *Lrig1*)[50–52] and general cell cycle regulators (for example, *Trp53* and *Cdkn2a*)[53,54] were enriched as knockouts that increase both young and old NSC activation (Fig. 1h,i and Supplementary Table 1).

Notably, a large fraction of gene knockouts increased activation only in young or only in old NSCs, which suggested that some NSC quiescence regulators change as a function of age. Some of the young-specific gene knockouts, such as *CREBBP*, are known to regulate NSC activation[55]. By contrast, many of the old-specific gene knockouts, such as *Sptlc2*, *Rsph3a* and, *Pxdc1* and the glucose transporter genes *Slc2a4* (which encodes GLUT4) and *Slc2a12* (which encodes GLUT12), had not been previously implicated in NSC activation (Fig. 1f–i and Extended Data Fig. 2a–c).

Gene ontology (GO) term analysis showed that gene knockouts that specifically boosted old NSC activation included those involved in cilium organization, cytoplasmic ribonucleoprotein structures (P-bodies and RNA-binding proteins) and glucose transport (Fig. 1m and Supplementary Table 2; see Extended Data Fig. 2d–g for genes that impede NSC activation). Primary cilia are linked to the quiescent state of NSCs[56], and knockout of primary cilia genes in young NSCs leads to decreased proliferation in mice[57–59], but their role in ageing NSCs was unknown. The GO term cytoplasmic ribonucleoprotein structures is notable, as cytoplasmic protein aggregates are observed in ageing qNSCs[25]. Glucose metabolism signatures have been linked to the quiescent state of NSCs[11,25,60,61], and regulation of glucose metabolism can affect young NSC self-renewal[62], survival[63] and differentiation to neurons[61,64,65]. However, glucose transport itself has not been previously implicated in NSC function during ageing, and more generally, the role of glucose metabolism in old NSCs is not known. Together, these results provide an exhaustive dataset with gene knockouts that restore the transition from quiescence to activation, a key aspect of neural stem cell ageing.

CRISPR–Cas9 screens in old brains

Primary cultures from old mice recapitulate several aspects of in vivo ageing but not all, and there are currently no methods to rapidly screen multiple genes for functional impact on ageing cells in vivo. To test whether gene knockouts can also boost NSC function in vivo, we developed a gene knockout screening platform for the ageing brain. The SVZ neurogenic region provides a good model for in vivo screening. qNSCs of the SVZ niche normally activate and produce progeny, which then migrate out of the niche to generate new neurons at a distal location in the olfactory bulb[4]. We leveraged the natural properties of this regenerative region to design a CRISPR–Cas9 screening platform in old mice. We performed stereotaxic brain surgery in old Cas9 mice to inject sgRNA-expressing and mCherry-expressing lentiviruses directly into the lateral ventricles, in close proximity to NSCs from the SVZ neurogenic niche (Fig. 2a). We verified that injection led to infection of NSCs in the niche through mCherry immunofluorescence and staining for markers of qNSCs ($GFAP^+Ki67^-$) and aNSCs ($GFAP^+Ki67^+$) (Fig. 2b and Extended Data Fig. 3a). After 5 weeks to allow time for both knockout to occur and NSC progeny to migrate to the olfactory bulb, we collected the entire olfactory bulb for genomic sequencing of sgRNAs (Fig. 2a). We verified that $mCherry^+$ cells (cells infected by the virus) were found in the olfactory bulb after 5 weeks (Extended Data Fig. 3b). We validated that injecting sgRNAs targeting eGFP in the SVZ niche of old Cas9 mice (which also express an eGFP reporter) led to decreased eGFP staining in the olfactory bulb after 5 weeks (Extended Data Fig. 3c,d). Notably, we also confirmed that sgRNAs targeting a specific gene (*Slc2a4*) led to decreased GLUT4 staining both in the SVZ and the olfactory bulb after 5 weeks (see Fig. 3a–d). Thus, stereotactic injection of lentiviruses with sgRNAs in lateral ventricles in vivo leads to efficient gene knockout in the SVZ niche and, after 5 weeks, results in lentivirus-infected cells with knockout in the olfactory bulb.

We verified the coverage and diversity of sgRNAs in vivo by injecting old Cas9 mice with lentivirus expressing 50 sgRNAs targeting the top 10 genes ('top 10' library) that specifically boosted old NSC activation from our first 2 in vitro screens (each gene targeted by 5 unique sgRNAs), and 100 negative control sgRNAs targeting unannotated regions of the genome (150 sgRNAs total). One day after injection, we extracted and sequenced genomic DNA from the SVZ niche and three distant brain regions: the olfactory bulb (where NSC progeny eventually migrate) and the outer cortex and the cerebellum as negative controls (regions where NSC progeny do not migrate) (Fig. 2c). At the day 1 timepoint, 150 sgRNAs were detected in the SVZ niche, and only a fraction of sgRNAs at 100–1,000-fold fewer sequencing reads were detected in the olfactory bulb, cerebellum and outer cortex (Fig. 2c and Extended Data Fig. 4a). Five weeks after injection (in a different old Cas9 mouse), we also collected the same brain regions (Fig. 2d). At the week 5 timepoint, 150 sgRNAs were again detected in the SVZ niche, but now the majority were also detected in the olfactory bulb, which suggested that NSCs containing sgRNAs had migrated out of the SVZ niche and allowed distal neurogenesis in the olfactory bulb (Fig. 2d and Extended Data Fig. 4b). The 50 sgRNAs targeting the top 10 gene pool were strongly enriched compare with the 100 control sgRNAs in the olfactory bulb, and to a lesser extent in the SVZ niche (Fig. 2c,d). The sgRNA abundance in the olfactory bulb is unlikely to be explained by the expansion of cells infected in the olfactory bulb itself given the lack of sgRNA diversity in the olfactory bulb at 1 day after infection (Fig. 2c and Extended Data Fig. 4a). Notably, we did not observe top 10 genes sgRNA pool enrichment over control in the cerebellum or cortex (negative control regions, Fig. 2d) or in wild-type mice that do not express Cas9 (Extended Data Fig. 4c). Hence, our in vivo platform leverages the natural properties of the NSC niche and the production of neurons in a distal region, which enabled efficient targeted CRISPR–Cas9 screening in vivo.

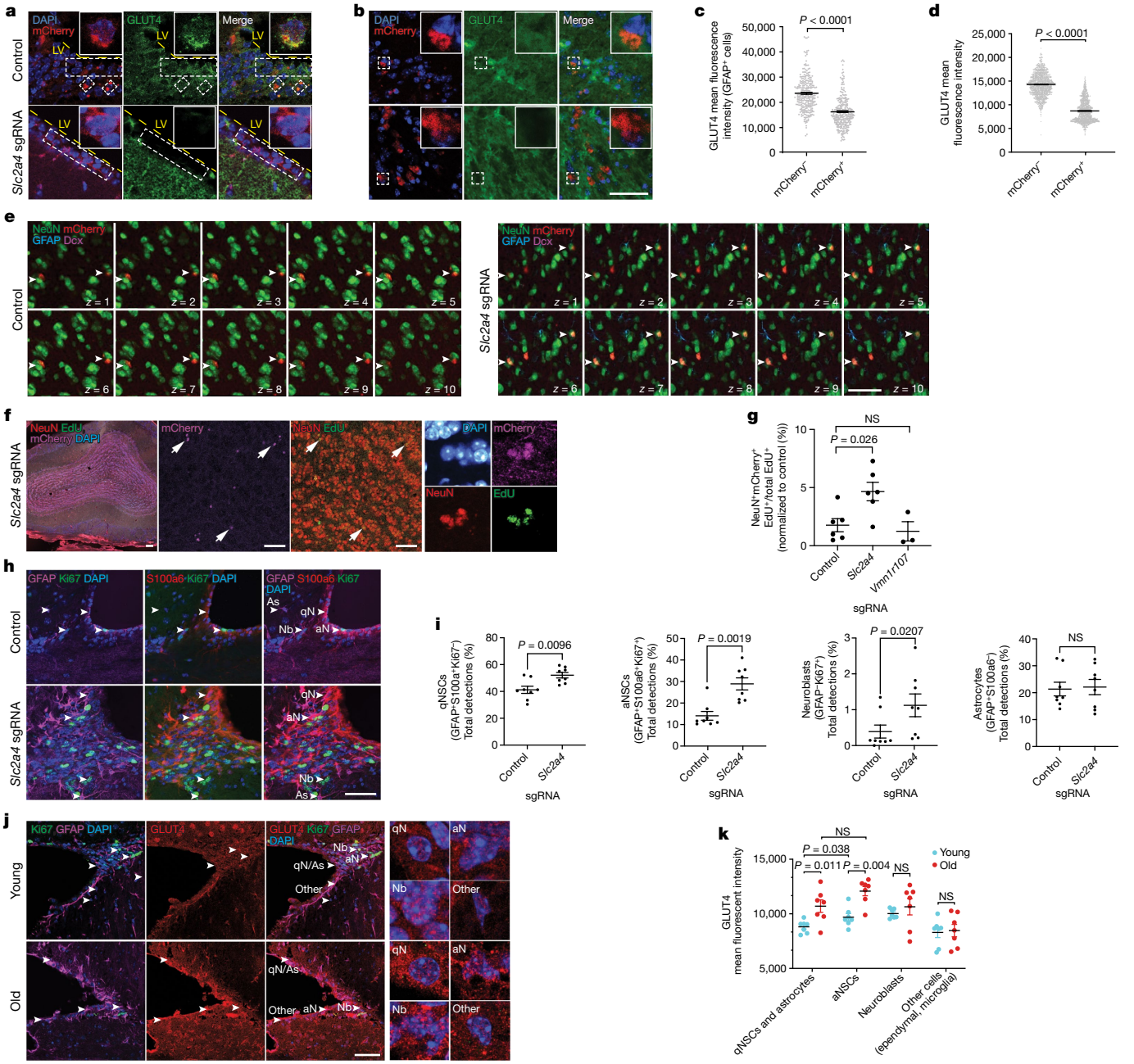

Fig. 3 | *Slc2a4* knockout in the SVZ NSC niche boosts neurogenesis in old mice. **a**,**b**, Immunofluorescence images of SVZ niche sections from old (21 months) female (**a**) or OB sections from old (22 months) male (**b**) Cas9 mice 5 weeks after injection of lentivirus expressing *Scl2a4* sgRNAs into the lateral ventricles (LVs). One experiment. mCherry (lentivirus-infected cells, red), GLUT4 (green), DAPI (blue). Dashed rectangles highlight examples of mCherry-infected cells. Insets, zoomed-in images. **c**,**d**, Quantification of GLUT4 mean fluorescence intensity in the SVZ (**c**) and the OB (**d**). Mean ± s.e.m. of GLUT4 fluorescence intensity for $n = 285$ mCherry$^-$ and $n = 285$ mCherry$^+$GFAP$^+$ cells (**c**) and $n = 1{,}333$ mCherry$^-$ and $n = 897$ mCherry$^+$ cells (**d**) in 1 old (22 month) Cas9 male mouse injected with *Slc2a4* sgRNAs. Each dot represents one cell. Two-tailed Mann–Whitney test. **e**,**f**, *z* stack confocal (**e**) and immunofluorescence (**f**) images of OB sections from old (20 months) male Cas9 mice 5 weeks after injection of lentivirus expressing control or *Slc2a4* sgRNAs into the LVs. Mice were injected with EdU once per week for 4 weeks, starting 1 week after virus injection. One experiment. **e**, NeuN (mature neurons, green), mCherry (lentivirus-infected cells, red), GFAP (astrocytes, blue), Dcx (neuroblasts, magenta). Arrowheads indicate lentivirus-infected NeuN$^+$ cells. *z* stack positions indicated on the bottom right. **f**, EdU (newborn cells, green), mCherry (lentivirus-infected cells, magenta), NeuN (mature neurons, red), DAPI (blue). Arrows indicate lentivirus-infected NeuN$^+$ cells. Right, zoomed-in images. **g**, Newborn neuron quantification in the OB. Mean ± s.e.m. of newborn neurons (NeuN$^+$mCherry$^+$EdU$^+$) average number over total EdU$^+$ cell number from 3 OB sections (normalized to control) for $n = 6$ (control), $n = 6$ (*Slc2a4*), $n = 3$ (*Vnm1r107*) old (18–21 months) male Cas9 mice, over 3 experiments. Each dot represents one mouse. Two-tailed Mann–Whitney test. **h**, Immunofluorescence images of SVZ sections from old (21 months) male Cas9 mice 5 weeks after injection of lentivirus expressing *Slc2a4* sgRNAs into the LVs. One experiment. Ki67 (green), GFAP (magenta), S100a6 (red), DAPI (blue). qNSCs (qN; GFAP$^+$S100a6$^+$Ki67$^-$), aNSCs (aN; GFAP$^+$S00a6$^+$Ki67$^+$), neuroblasts (Nb; GFAP$^-$Ki67$^+$), astrocytes (As; GFAP$^+$S100a6$^-$). **i**, Quantification of qNSC, aNSC, neuroblast and astrocyte number in the SVZ. Mean ± s.e.m. of average cell number from about 8 SVZ sections for $n = 8$ (control) and $n = 8$ (*Slc2a4*) old (18–21 months) male Cas9 mice, over 3 experiments. Each dot represents one mouse. Two-tailed Mann–Whitney test. **j**, Immunofluorescence images of GLUT4 levels in SVZ sections from young (3–4 months) and old (18–21 months) male Cas9 mice. One experiment. GLUT4 (red), Ki67 (green), GFAP (magenta), DAPI (blue). qNSC and astrocytes (GFAP$^+$Ki67$^-$), aNSCs (GFAP$^+$Ki67$^+$), neuroblasts (GFAP$^-$Ki67$^+$), other cells (GFAP$^-$Ki67$^-$). Right, zoomed-in images. **k**, Quantification of GLUT4 mean fluorescence intensity in the SVZ niche. Cell types as in **j**. Mean ± s.e.m. of GLUT4 mean fluorescence intensity for $n = 7$ (young) and $n = 7$ (old) male Cas9 mice, over 2 experiments. Each dot represents one mouse. Two tailed Mann–Whitney test. Scale bars, 50 µm (**a**,**b**,**e**,**f** (middle and right), **j**) or 100 µm (**f** (left), **h**).

Using this platform, we performed three independent targeted screens in old Cas9 mice, each assessing five libraries of 10 genes for their ability to boost NSC activation and migration to the olfactory bulb. In addition to the top 10 gene library, we selected four other sets of 10 genes based on our genome-wide screens in cultured NSCs. The following five libraries were generated: (1) 'top 10' library, with genes that when knocked out boosted old NSC activation in our in vitro screens (screens 1 and 2) (for example, *Rsph3a*); (2) 'glucose uptake/human disease' library, with genes that when knocked out also boosted activation of old NSCs in our in vitro screens (for example, *Slc2a4*, *Slc2a12* and *Sorl1*); (3) 'cytoplasmic ribonucleoprotein structures' library, with genes that belong to the P-bodies and cytoplasmic ribonucleoprotein/stress granule GO terms, some of which boosted old NSC activation in our in vitro screen (for example, *Dis3l2*, *Mbnl1* and *Edc3*); (4) 'depleted (young/old)' library, with genes that when knocked out blocked young or old NSC activation in our in vitro screens (screens 1 and 2); and (5) 'published NSC regulators' library, with genes that have previously been implicated in NSC function in the literature (Fig. 2e). We injected old Cas9 mice with virus to express one of the 5 libraries along with the 100 control sgRNA library, waited 5 weeks and then sequenced sgRNAs in the olfactory bulbs and performed CasTLE analysis (Fig. 2e). Of the 50 gene knockouts tested, we identified 24 gene knockouts that were significantly enriched in the olfactory bulb in 1 of the in vivo screens, with 7 higher-confidence knockouts significantly enriched in at least 2 out of 3 screens (Fig. 2e–g and Extended Data Fig. 4d–g). These data suggest that these knockouts boost old NSC activation (and/or migration and differentiation) (for example, *Rsph3a*, *Sorl1* and *Slc2a4*) (Fig. 2e,f and Extended Data Fig. 4d,e,g; see Fig. 3 for an independent validation of *Slc2a4*). Of the 10 gene knockouts predicted to impede NSC activation, the four predicted to specifically block old NSC activation were slightly but not significantly depleted in the olfactory bulb (Fig. 2e,g and Extended Data Fig. 4f). The lack of sensitivity in detecting gene knockouts that are depleted in the olfactory bulb may be due to the low levels of neurogenesis in old mice. In support of this idea, significant depletion of some of these gene knockouts was observed in young mice (Extended Data Fig. 4h). Of the nine published NSC regulators that had a significant effect in in vivo screens, three had the same effect in in vitro screens (Extended Data Fig. 4i), which suggested that in vivo screens can identify some genes that are missed in vitro, perhaps due to differences in cell cycle status or cell–matrix interactions. Notably, of the activating gene knockouts tested based on our in vitro screens, some of the most enriched gene knockouts were associated with cilia (*Rsph3a*), glucose uptake (*Slc2a4* and *Slc45a4*) and Alzheimer's disease (*Sorl1*) (Fig. 2e). The 'glucose uptake/human disease' library was most strongly enriched, with nine out of the 10 gene knockouts reaching significance in at least one in vivo screen (Fig. 2e). Overall, these data establish a scalable platform to genetically screen in vivo for genes that affect old NSC function and highlight the importance of cilia, glucose metabolism and ribonucleoprotein structures for ageing NSCs.

Knocking out GLUT4 boosts neurogenesis

One of the most consistent gene knockouts that boost old NSC function both in vitro and in vivo is *Slc2a4* knockout. GLUT4 is an insulin-dependent glucose transporter[66]. Glucose metabolism has been previously implicated in young NSC self-renewal[62], survival[63] and differentiation[61,64,65], but the importance of the key step of glucose import in NSC function is unclear. More generally, the role of glucose metabolism in old NSCs is not known. We asked whether reducing GLUT4 in the SVZ niche is sufficient to boost the ability of NSCs to generate newborn neurons in the olfactory bulb (neurogenesis) in old individuals. To this end, we stereotactically injected sgRNAs targeting *Slc2a4* into the ventricles of old Cas9 mice (Extended Data Fig. 5a). As two types of negative control, we used sgRNAs to unannotated regions of the genome (control) or sgRNAs targeting *Vmn1r107*, a gene that was depleted in in vitro screens but did not have a significant effect in in vivo screens (Fig. 2e and Extended Data Fig. 2d). We verified that sgRNAs targeting *Slc2a4* successfully reduced GLUT4 staining in the SVZ (Fig. 3a,c) and the olfactory bulb (Fig. 3b,d) 5 weeks after injection of lentivirus in the SVZ NSC niche. To track newborn cells arriving in the olfactory bulb, we injected mice weekly starting 7 days after virus injection with 5-ethynyl-2′-deoxyuridine (EdU), a thymidine analogue that incorporates into newly synthesized DNA and can be visualized by immunofluorescent assays (Fig. 3e–g and Extended Data Fig. 5b–d). We first quantified the number of newborn cells in the olfactory bulb 5 weeks after virus injection by co-staining for EdU (newborn cells) and mCherry (sgRNA lentivirus reporter) (Extended Data Fig. 5b–d). *Slc2a4* knockout resulted in a greater than twofold increase in the proportion of newborn cells that were $mCherry^+$ relative to control treatment in the olfactory bulb (Extended Data Fig. 5b–d). We then assessed whether cells with *Slc2a4* knockout differentiated into neurons by staining for neuronal markers (TUJ1 and NeuN). Most cells targeted by the *Slc2a4* sgRNA ($mCherry^+$) were positive for the neuronal nucleus marker (NeuN) in the olfactory bulb (Fig. 3e–g and Extended Data Fig. 5e,f). Notably, *Slc2a4* knockout in the SVZ resulted in a significant increase in the number of newborn neurons ($NeuN^+EdU^+$ cells) in the olfactory bulb (Fig. 3g). Cells with *Slc2a4* knockout were also positive for the neuronal marker TUJ1 (and a few cells were positive for the mature neuron marker calretinin) (Extended Data Fig. 5g–i). By contrast, cells with *Slc2a4* knockout were negative for markers of neuroblasts (Dcx), astrocytes (GFAP) or oligodendrocytes (OLIG2 and SOX10) in the olfactory bulb (Extended Data Fig. 5j). These results suggest that *Slc2a4* knockout in the SVZ niche improves neurogenesis.

We next tested whether the enhanced neurogenesis observed for *Slc2a4* knockout was accompanied by increased NSC numbers in the SVZ niche. Immunofluorescence experiments with markers of SVZ niche NSCs[67] showed that *Slc2a4* knockout led to an increased number of qNSCs ($GFAP^+S100a6^+Ki67^-$), aNSCs ($GFAP^+S100a6^+Ki67^+$) and neuroblasts ($GFAP^-Ki67^+$) (Fig. 3h,i). The enhanced number of qNSCs in *Slc2a4* knockout brains could be due to increased symmetric division followed by return to quiescence[68,69]. There was no NSC exhaustion in the niche after *Slc2a4* knockout, at least at this 5 week timepoint. Thus, increased neurogenesis after *Slc2a4* knockout is accompanied by enhanced NSC number in vivo.

Given the beneficial effect of GLUT4 depletion in old NSCs in vivo, we asked whether GLUT4 expression itself changes in the SVZ neurogenic niche with age. We performed immunofluorescence staining of GLUT4 in SVZ sections from young and old mice followed by quantification using an automated pipeline (see Methods). GLUT4 was increased in astrocytes and in qNSCs ($GFAP^+Ki67^-$) (and in aNSCs and in neural progenitor cells (NPCs); $GFAP^+Ki67^+$) in the old brain (Fig. 3j,k and Extended Data Fig. 5k), although the increase was not large. By contrast, GLUT4 expression did not change with age in other cell types (ependymal or microglia; $GFAP^-Ki67^-$) (Fig. 3j,k and Extended Data Fig. 5k). Analysis of single-cell RNA sequencing data[70] showed that *Slc2a4* transcripts increased with age in qNSCs and in astrocytes, but not in other cell types (Extended Data Fig. 5l), which might underlie some of the changes in GLUT4 levels with age. Immunofluorescence staining and quantification using S100a6, a marker that is relatively specific to SVZ niche NSCs[67], corroborated the increase in GLUT4 in old NSCs (Extended Data Fig. 5m,n). Thus, expression of the glucose transporter GLUT4 increases during ageing in NSCs in vivo, and knockout of this transporter boosts NSC number and neurogenesis in old mice. Together, these data raise the possibility that the age-dependent increase in GLUT4 could be detrimental for NSC function and neurogenesis in old brains.

Old NSCs exhibit high glucose uptake

GLUT4 is a transporter that increases glucose uptake in an insulin-dependent manner in cells[66] (Fig. 4a). We therefore assessed

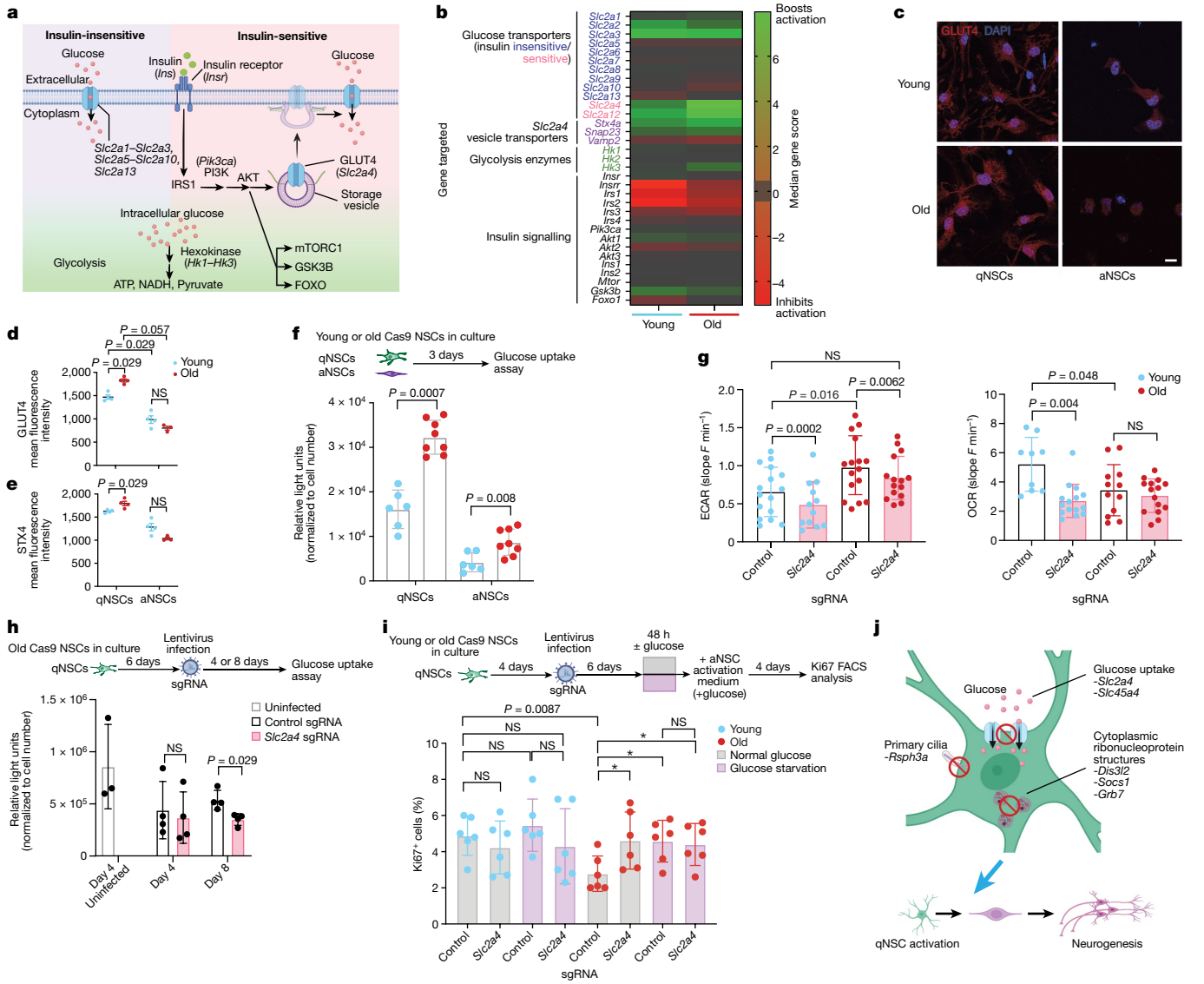

Fig. 4 | Old NSCs exhibit high glucose uptake that can be targeted to improve activation. a, Glucose uptake pathway. **b**, Heatmap plotting glucose and insulin pathway median gene scores from genome-wide in vitro screens (day 4). Gene knockouts that boost (green) or impede (red) NSC activation. **c**, Immunofluorescence image of GLUT4 staining in cultured qNSCs and aNSCs from young (3–4 months) and old (18–21 months) Cas9 mice (mixed sex). GLUT4 (red), DAPI (blue). One experiment. Scale bar, 10 µm. **d**,**e**, Quantification of GLUT4 (**d**) and STX4A (**e**) mean fluorescence. Mean ± s.e.m. of mean fluorescence for $n = 4$ (young qNSCs, old qNSCs, young aNSCs) and $n = 3$ (old aNSCs) cultures, each from six pooled Cas9 mice (three males, three females). One experiment. Each dot represents one NSC culture. Two-tailed Mann–Whitney test. **f**, Schematic (top) and quantification (bottom) of bioluminescent glucose uptake in primary qNSCs and aNSCs from young and old mice. Mean ± s.e.m. of results for $n = 6$ (young qNSCs, aNSCs) and $n = 8$ (old qNSCs, aNSCs) cultures, each from six pooled Cas9 mice (three males, three females), over two experiments. Each dot represents one NSC culture. Two-tailed Mann–Whitney test. **g**, ECAR and OCR in qNSCs from young and old mice. qNSCs infected with control or *Slc2a4* sgRNAs lentiviruses. ECAR, mean ± s.d. of results for $n = 16$ (young and old, control), $n = 12$ (young, *Slc2a4*) and $n = 15$ (young, *Slc2a4*) NSC cultures, each from two pooled mice (one male, one female), over two experiments. OCR, mean ± s.d. of results for $n = 9$ (young, control), $n = 15$ (young and old, *Slc2a4*) and $n = 12$ (old, control) NSC cultures, each from two pooled Cas9 mice (one male, one female), over two experiments. Each dot represents one NSC culture. One-tailed Wilcoxon signed-rank test (within age groups), one-tailed Mann–Whitney test (across age groups). **h**, Schematic (top) and quantification (bottom) of bioluminescent glucose uptake in primary qNSC cultures from old mice. qNSCs infected with *Slc2a4* or control sgRNAs lentiviruses, or uninfected, were assessed for glucose uptake at day 4 or day 8. Mean ± s.d. of results for $n = 3$ (uninfected), $n = 4$ (day 4) and $n = 5$ (day 8) NSC cultures, each from six pooled Cas9 mice (three males, three females), over two experiments. Each dot represents one NSC culture. Two-tailed Mann–Whitney test. **i**, Schematic (top) and quantification (bottom) of NSC activation efficiency for young and old qNSCs (FACS). qNSCs infected with control or *Slc2a4* sgRNAs lentiviruses were placed in quiescence medium with (grey) or without (pink) glucose for 2 days, then in activation medium (with glucose) for 4 days. Mean ± s.d. of $Ki67^+$ cell percentage for $n = 6$ NSC cultures (each condition), each from six pooled Cas9 mice (three males, three females), over two experiments. Each dot represents one NSC culture. Two-tailed Mann–Whitney test. *P* values in source data. **j**, Summary of gene knockout interventions that boost old NSC activation in both in vitro and in vivo screens. The models in **a** and **j** were created using BioRender (https://biorender.com).

components of the glucose uptake pathway (insulin-dependent or independent) in the context of NSC ageing by mining our genome-wide in vitro screen results. Among the 12 known glucose transporters in mice, only *Slc2a4* and *Slc2a12*, when knocked out, significantly boosted old NSC activation in vitro (Fig. 4a,b). In vivo, *Slc2a4* knockout (but not *Scl2a12* knockout) improved neurogenesis in old mice (Figs. 2 and 3).

Furthermore, analysis of single-cell RNA sequencing data[70] showed that among the 12 glucose transporters, only *Slc2a4* was significantly upregulated in qNSCs during ageing (Extended Data Fig. 6a). Immunofluorescence staining of GLUT4 in NSC cultures from young and old mice, followed by automated quantification, indicated that GLUT4 levels were increased in old qNSCs (although this increase was not large) (Fig. 4c,d), consistent with the in vivo observations (Fig. 3j,k and Extended Data Fig. 5l). By contrast, age-dependent GLUT4 levels were not consistent in vitro and in vivo in aNSCs (Figs. 3j,k and 4c,d and Extended Data Fig. 6e), perhaps owing to cell cycle heterogeneity or cell–matrix interactions. Hence, among the different glucose transporters, GLUT4 may particularly affect qNSC function during ageing.

Within the glucose uptake pathway, knockout of *Stx4a*, which encodes a protein that facilitates the fusion of GLUT4 storage vesicles with the plasma membrane[66] (among other functions), boosted old NSC activation in one of the screens (Fig. 4b). Immunofluorescence staining, followed by unbiased quantification, indicated that STX4A was also increased in old qNSCs in vitro and in vivo, although this increase was not large (Fig. 4e and Extended Data Fig. 6b–d). By contrast, proteins in the glycolysis, insulin and associated downstream pathways (for example, hexokinase enzymes HK1–HK3, mTOR, GSK3B and FOXO) were not enriched in the genome-wide screens in old NSCs, and some insulin pathway genes were even depleted (Fig. 4a,b). Collectively, these observations suggest that glucose transporter activity could be a key step in regulating old NSC activation.

We next asked whether glucose uptake changes with age in NSCs. Two independent glucose uptake assays showed that old qNSCs and aNSCs in culture take up about twofold more glucose than their young counterparts (Fig. 4f and Extended Data Fig. 6f). The increase in glucose uptake in old qNSCs, coupled with the reduction in glucose uptake after *Slc2a4* knockout in these cells (Fig. 4h), is consistent with the slight increase in GLUT4 levels observed by immunofluorescence staining in vitro and in vivo in old qNSCs.

To determine whether the age-dependent increase in glucose uptake affects downstream metabolic pathways in qNSCs, we measured the extracellular acidification rate (ECAR), which mostly reflects glycolysis, and the oxygen consumption rate (OCR), which reflects mitochondrial respiration[71]. Old qNSCs had a significantly higher ECAR and lower OCR compared with young counterparts (Fig. 4g), which suggested that old qNSCs have higher glycolysis and decreased respiration. Moreover, analysis of single-cell RNA sequencing data[70] indicated that a gene expression signature for fatty acid oxidation (FAO), a process that is normally high in young qNSCs[72], decreased with age in qNSCs (Extended Data Fig. 6g). Thus, old qNSCs may increase their usage of glucose (compared with other sources) for energy metabolism. *Slc2a4* knockout significantly decreased both ECAR and OCR in young qNSCs (Fig. 4g). By contrast, *Slc2a4* knockout decreased only ECAR (and not OCR) in old qNSCs (Fig. 4g). These results raise the possibility that GLUT4 depletion boosts old NSC activation in part by reducing glycolysis.

We then determined whether restricting glucose uptake, either genetically or by depleting glucose in the medium, promotes the activation of old NSCs. We verified that individual *Slc2a4* knockout was efficient in qNSCs both at the genomic and protein level (Extended Data Fig. 6h–m) and that it significantly reduced glucose uptake in old qNSCs (Fig. 4h). We then tested the effect of *Slc2a4* knockout on the ability of qNSCs to activate. In line with our screen results, individual *Slc2a4* knockout improved the ability of old (but not young) qNSCs to transition from quiescence to activation (Fig. 4i and Extended Data Fig. 6n). A brief 48-h pulse of glucose starvation in qNSCs improved the ability of old (but not young) qNSCs to activate (Fig. 4i and Extended Data Fig. 6n). GLUT4 depletion did not further increase old qNSC activation in the context of a pulse of glucose starvation (Fig. 4i and Extended Data Fig. 6n), which suggests that one mechanism by which GLUT4 reduction improves old NSC activation is by lowering glucose. Consistently, treatment with 2-deoxy-D-glucose (2-DG), a glucose analogue that cannot undergo glycolysis, boosted old (but not young) qNSC activation (Extended Data Fig. 6o). Together, these data show that old qNSCs are in a state of high glucose uptake, probably because of increased GLUT4 expression during ageing. However, this can be reversed through genetic or glucose restriction perturbations to promote old qNSC activation. These results highlight the use of genetic screens in old cells to uncover genetic pathways (for example, glucose metabolism, primary cilia and ribonucleoprotein structures) and interventions to boost NSC function during ageing (Fig. 4j).

Discussion

This study used genome-wide knockout screens to identify genes that affect ageing in a regenerative neurogenic niche. We also developed a CRISPR–Cas9 targeted screening platform to study functional regulators of cellular ageing in vivo. The power of knockout screens is their ability to uncover new biology. Here we identified more than 300 genes that when knocked out in the context of genome-wide screen boost the activation of old NSCs in vitro, and 10 out of 10 of the top genes individually validate. The genes uncovered by the screen include glucose metabolism, ribonucleoprotein structures, and primary cilia-associated genes as well as many others. Most of these genes had not previously been identified to regulate NSCs, especially old NSCs, and they represent a resource for functional regulators of NSC ageing and rejuvenation, although it will be important to further validate these genes through individual knockouts. It will also be interesting to test overexpression of genes whose knockouts specifically impede young cells. Given the spatial heterogeneity of NSCs in the SVZ niche[13,73,74], assessing how gene knockouts affect NSCs in a spatially restricted manner could uncover interactions between select genes and spatial location.

The knockout of the insulin-sensitive glucose transporter GLUT4 was consistently a top hit for both in vitro and in vivo screens, which led to a twofold increase in neurogenesis in old mice in vivo. Old qNSCs exhibited an increase in glucose uptake, with two times more glucose uptake than their young counterparts. Reversing this increase, either genetically or by glucose starvation, boosted the ability of old (but not young) NSCs to activate. By contrast, manipulating other glucose transporters does not have a strong effect on NSC activation. The importance of GLUT4 among other glucose transporters in regulating NSC ageing could be due to the slight increase in GLUT4 levels with age or the insulin-dependency of this glucose transporter[66]. As the age-dependent changes in GLUT4 expression are not large, other factors could indeed contribute to the selectivity of old NSCs to *Scl2a4* knockout. It will be interesting to test the role of age-dependent insulin resistance or specific syntaxins (for example, STX4A) in regulating glucose uptake during ageing. More generally, gene network differences between NSCs at different ages could underlie the specific sensitivity of young and old NSCs to some of the gene knockouts.

The way in which increased glucose impedes NSCs could involve metabolic regulation downstream of glycolysis or other processes that use glucose. It will be interesting to examine changes in various metabolic substrates NSCs could use (for example, fatty acids) during ageing. Other stem cells, including haematopoietic stem cells and muscle stem cells, display greater glucose usage and higher levels of glycolysis with age in mice and humans[75,76], although the functional consequences of these metabolic changes have not yet been tested. In addition, glucose restriction extends lifespan in yeast[77] and worms[78,79], whereas high glucose shortens worm lifespan[80,81]. Thus, increased glucose levels may be a general feature of cell and organismal ageing. Dysregulated insulin–glucose signalling has also been linked to neuronal dysfunction and human brain ageing and Alzheimer's disease[82]. Our discovery that the increased glucose uptake in old cells can be targeted with GLUT4 knockout or glucose restriction raises the possibility that such mechanism could be targeted more broadly to counter ageing.

Systemic gene therapy interventions can rejuvenate aspects of ageing in progeria or even physiologically old mice[37,83,84]. A major challenge has been to rapidly identify new genetic interventions to counter ageing in vivo. The establishment of an in vivo screening platform shows a relatively high-throughput and rapid method of testing genetic interventions in the context of a regenerative stem cell niche in vivo. This type of screen should be scalable, versatile to use with other CRISPR–Cas9 techniques (for example, gene activation or inhibition), and applicable to other cell types (for example, other stem cells) in old mice. Genetic interventions that impact old tissues have the potential to identify new strategies—genetic or environmental—to delay or reverse features of ageing. In the brain, such interventions can be particularly important to counter cognitive and regenerative decline during ageing and neurodegenerative diseases.

Online content

Any methods, additional references, Nature Portfolio reporting summaries, source data, extended data, supplementary information, acknowledgements, peer review information; details of author contributions and competing interests; and statements of data and code availability are available at https://doi.org/10.1038/s41586-024-07972-2.

1. Gage, F. H. & Temple, S. Neural stem cells: generating and regenerating the brain. *Neuron* **80**, 588–601 (2013).
2. Silva-Vargas, V., Crouch, E. E. & Doetsch, F. Adult neural stem cells and their niche: a dynamic duo during homeostasis, regeneration, and aging. *Curr. Opin. Neurobiol.* **23**, 935–942 (2013).
3. Navarro Negredo, P., Yeo, R. W. & Brunet, A. Aging and rejuvenation of neural stem cells and their niches. *Cell Stem Cell* **27**, 202–223 (2020).
4. Bond, A. M., Ming, G. L. & Song, H. Adult mammalian neural stem cells and neurogenesis: five decades later. *Cell Stem Cell* **17**, 385–395 (2015).
5. Yousef, H. et al. Age-associated increase in BMP signaling inhibits hippocampal neurogenesis. *Stem Cells* **33**, 1577–1588 (2015).
6. Chaker, Z., Aid, S., Berry, H. & Holzenberger, M. Suppression of IGF-I signals in neural stem cells enhances neurogenesis and olfactory function during aging. *Aging Cell* **14**, 847–856 (2015).
7. Molofsky, A. V. et al. Increasing *p16*^{INK4a} expression decreases forebrain progenitors and neurogenesis during ageing. *Nature* **443**, 448–452 (2006).
8. Bedrosian, T. A. et al. Lamin B1 decline underlies age-related loss of adult hippocampal neurogenesis. *EMBO J.* **40**, e105819 (2021).
9. Arvidsson, A., Collin, T., Kirik, D., Kokaia, Z. & Lindvall, O. Neuronal replacement from endogenous precursors in the adult brain after stroke. *Nat. Med.* **8**, 963–970 (2002).
10. Doetsch, F., Caille, I., Lim, D. A., Garcia-Verdugo, J. M. & Alvarez-Buylla, A. Subventricular zone astrocytes are neural stem cells in the adult mammalian brain. *Cell* **97**, 703–716 (1999).
11. Llorens-Bobadilla, E. et al. Single-cell transcriptomics reveals a population of dormant neural stem cells that become activated upon brain injury. *Cell Stem Cell* **17**, 329–340 (2015).
12. Jin, K. et al. Evidence for stroke-induced neurogenesis in the human brain. *Proc. Natl Acad. Sci. USA* **103**, 13198–13202 (2006).
13. Obernier, K. & Alvarez-Buylla, A. Neural stem cells: origin, heterogeneity and regulation in the adult mammalian brain. *Development* **146**, dev156059 (2019).
14. Shin, J. et al. Single-cell RNA-seq with Waterfall reveals molecular cascades underlying adult neurogenesis. *Cell Stem Cell* **17**, 360–372 (2015).
15. Luo, J., Daniels, S. B., Lennington, J. B., Notti, R. Q. & Conover, J. C. The aging neurogenic subventricular zone. *Aging Cell* **5**, 139–152 (2006).
16. Mirzadeh, Z., Merkle, F. T., Soriano-Navarro, M., Garcia-Verdugo, J. M. & Alvarez-Buylla, A. Neural stem cells confer unique pinwheel architecture to the ventricular surface in neurogenic regions of the adult brain. *Cell Stem Cell* **3**, 265–278 (2008).
17. Shen, Q. et al. Adult SVZ stem cells lie in a vascular niche: a quantitative analysis of niche cell–cell interactions. *Cell Stem Cell* **3**, 289–300 (2008).
18. Tavazoie, M. et al. A specialized vascular niche for adult neural stem cells. *Cell Stem Cell* **3**, 279–288 (2008).
19. Enwere, E. et al. Aging results in reduced epidermal growth factor receptor signaling, diminished olfactory neurogenesis, and deficits in fine olfactory discrimination. *J. Neurosci.* **24**, 8354–8365 (2004).
20. Tropepe, V., Craig, C. G., Morshead, C. M. & van der Kooy, D. Transforming growth factor-α null and senescent mice show decreased neural progenitor cell proliferation in the forebrain subependyma. *J. Neurosci.* **17**, 7850–7859 (1997).
21. Ibrayeva, A. et al. Early stem cell aging in the mature brain. *Cell Stem Cell* **28**, 955–966 e957 (2021).
22. Bondolfi, L., Ermini, F., Long, J. M., Ingram, D. K. & Jucker, M. Impact of age and caloric restriction on neurogenesis in the dentate gyrus of C57BL/6 mice. *Neurobiol. Aging* **25**, 333–340 (2004).
23. Gheusi, G. & Lledo, P. M. Adult neurogenesis in the olfactory system shapes odor memory and perception. *Prog. Brain Res.* **208**, 157–175 (2014).
24. Gontier, G. et al. Tet2 rescues age-related regenerative decline and enhances cognitive function in the adult mouse brain. *Cell Rep.* **22**, 1974–1981 (2018).
25. Leeman, D. S. et al. Lysosome activation clears aggregates and enhances quiescent neural stem cell activation during aging. *Science* **359**, 1277–1283 (2018).
26. Horowitz, A. M. et al. Blood factors transfer beneficial effects of exercise on neurogenesis and cognition to the aged brain. *Science* **369**, 167–173 (2020).
27. McAvoy, K. M. et al. Modulating neuronal competition dynamics in the dentate gyrus to rejuvenate aging memory circuits. *Neuron* **91**, 1356–1373 (2016).
28. Morgens, D. W., Deans, R. M., Li, A. & Bassik, M. C. Systematic comparison of CRISPR/Cas9 and RNAi screens for essential genes. *Nat. Biotechnol.* **34**, 634–636 (2016).
29. Morgens, D. W. et al. Genome-scale measurement of off-target activity using Cas9 toxicity in high-throughput screens. *Nat. Commun.* **8**, 15178 (2017).
30. Lytle, N. K. et al. A multiscale map of the stem cell state in pancreatic adenocarcinoma. *Cell* **177**, 572–586.e22 (2019).
31. Wang, T. et al. Gene essentiality profiling reveals gene networks and synthetic lethal interactions with oncogenic Ras. *Cell* **168**, 890–903.e15 (2017).
32. Kramer, N. J. et al. CRISPR–Cas9 screens in human cells and primary neurons identify modifiers of C9ORF72 dipeptide-repeat-protein toxicity. *Nat. Genet.* **50**, 603–612 (2018).
33. Tian, R. et al. Genome-wide CRISPRi/a screens in human neurons link lysosomal failure to ferroptosis. *Nat. Neurosci.* **24**, 1020–1034 (2021).
34. Shifrut, E. et al. Genome-wide CRISPR screens in primary human T cells reveal key regulators of immune function. *Cell* **175**, 1958–1971.e15 (2018).
35. Kamber, R. A. et al. Inter-cellular CRISPR screens reveal regulators of cancer cell phagocytosis. *Nature* **597**, 549–554 (2021).
36. Chow, R. D. et al. AAV-mediated direct in vivo CRISPR screen identifies functional suppressors in glioblastoma. *Nat. Neurosci.* **20**, 1329–1341 (2017).
37. Wang, W. et al. A genome-wide CRISPR-based screen identifies KAT7 as a driver of cellular senescence. *Sci. Transl. Med.* **13**, eabd2655 (2021).
38. Zheng, X. et al. Massively parallel in vivo Perturb-seq reveals cell-type-specific transcriptional networks in cortical development. *Cell* **187**, 3236–3248.e21 (2024).
39. Kalebic, N. et al. CRISPR/Cas9-induced disruption of gene expression in mouse embryonic brain and single neural stem cells in vivo. *EMBO Rep.* **17**, 338–348 (2016).
40. Beronja, S. & Fuchs, E. RNAi-mediated gene function analysis in skin. *Methods Mol. Biol.* **961**, 351–361 (2013).
41. Keys, H. R. & Knouse, K. A. Genome-scale CRISPR screening in a single mouse liver. *Cell Genom.* **2**, 100217 (2022).
42. Wertz, M. H. et al. Genome-wide in vivo CNS screening identifies genes that modify CNS neuronal survival and mHTT toxicity. *Neuron* **106**, 76–89.e8 (2020).
43. Ramani, B. et al. Scalable, cell type-selective, AAV-based in vivo CRISPR screening in the mouse brain. Preprint at *bioRxiv* https://doi.org/10.1101/2023.06.13.544831 (2023).
44. Bajaj, J. et al. An in vivo genome-wide CRISPR screen identifies the RNA-binding protein Staufen2 as a key regulator of myeloid leukemia. *Nat. Cancer* **1**, 410–422 (2020).
45. Rogers, Z. N. et al. Mapping the in vivo fitness landscape of lung adenocarcinoma tumor suppression in mice. *Nat. Genet.* **50**, 483–486 (2018).
46. Yamauchi, T. et al. Genome-wide CRISPR–Cas9 screen identifies leukemia-specific dependence on a pre-mRNA metabolic pathway regulated by DCPS. *Cancer Cell* **33**, 386–400.e5 (2018).
47. Wang, G. et al. Mapping a functional cancer genome atlas of tumor suppressors in mouse liver using AAV-CRISPR-mediated direct in vivo screening. *Sci. Adv.* **4**, eaao5508 (2018).
48. Martynoga, B. et al. Epigenomic enhancer annotation reveals a key role for NFIX in neural stem cell quiescence. *Genes Dev.* **27**, 1769–1786 (2013).
49. Platt, R. J. et al. CRISPR–Cas9 knockin mice for genome editing and cancer modeling. *Cell* **159**, 440–455 (2014).
50. Mira, H. et al. Signaling through BMPR-IA regulates quiescence and long-term activity of neural stem cells in the adult hippocampus. *Cell Stem Cell* **7**, 78–89 (2010).
51. Marques-Torrejon, M. A. et al. LRIG1 is a gatekeeper to exit from quiescence in adult neural stem cells. *Nat. Commun.* **12**, 2594 (2021).
52. Pineda, J. R. et al. Vascular-derived TGF-β increases in the stem cell niche and perturbs neurogenesis during aging and following irradiation in the adult mouse brain. *EMBO Mol. Med.* **5**, 548–562 (2013).
53. Satyanarayana, A. & Kaldis, P. Mammalian cell-cycle regulation: several CDKs, numerous cyclins and diverse compensatory mechanisms. *Oncogene* **28**, 2925–2939 (2009).
54. Hafner, A., Bulyk, M. L., Jambhekar, A. & Lahav, G. The multiple mechanisms that regulate p53 activity and cell fate. *Nat. Rev. Mol. Cell Biol.* **20**, 199–210 (2019).
55. Schoof, M. et al. The transcriptional coactivator and histone acetyltransferase CBP regulates neural precursor cell development and migration. *Acta Neuropathol. Commun.* **7**, 199 (2019).
56. Khatri, P. et al. Proliferation and cilia dynamics in neural stem cells prospectively isolated from the SEZ. *Sci. Rep.* **4**, 3803 (2014).
57. Tong, C. K. et al. Primary cilia are required in a unique subpopulation of neural progenitors. *Proc. Natl Acad. Sci. USA* **111**, 12438–12443 (2014).
58. Breunig, J. J. et al. Primary cilia regulate hippocampal neurogenesis by mediating sonic hedgehog signaling. *Proc. Natl Acad. Sci. USA* **105**, 13127–13132 (2008).
59. Han, Y. G. et al. Hedgehog signaling and primary cilia are required for the formation of adult neural stem cells. *Nat. Neurosci.* **11**, 277–284 (2008).
60. Knobloch, M. & Jessberger, S. Metabolism and neurogenesis. *Curr. Opin. Neurobiol.* **42**, 45–52 (2017).
61. Lange, C. et al. Relief of hypoxia by angiogenesis promotes neural stem cell differentiation by targeting glycolysis. *EMBO J.* **35**, 924–941 (2016).
62. Fusco, S. et al. A CREB–Sirt1–Hes1 circuitry mediates neural stem cell response to glucose availability. *Cell Rep.* **14**, 1195–1205 (2016).
63. Candelario, K. M., Shuttleworth, C. W. & Cunningham, L. A. Neural stem/progenitor cells display a low requirement for oxidative metabolism independent of hypoxia inducible factor-1α expression. *J. Neurochem.* **125**, 420–429 (2013).
64. Chen, X. et al. High glucose inhibits neural stem cell differentiation through oxidative stress and endoplasmic reticulum stress. *Stem Cells Dev.* **27**, 745–755 (2018).
65. Zhou, W. et al. TIGAR promotes neural stem cell differentiation through acetyl-CoA-mediated histone acetylation. *Cell Death Dis.* **10**, 198 (2019).

66. Leto, D. & Saltiel, A. R. Regulation of glucose transport by insulin: traffic control of GLUT4. *Nat. Rev. Mol. Cell Biol.* **13**, 383–396 (2012).
67. Kjell, J. et al. Defining the adult neural stem cell niche proteome identifies key regulators of adult neurogenesis. *Cell Stem Cell* **26**, 277–293 e278 (2020).
68. Obernier, K. et al. Adult neurogenesis is sustained by symmetric self-renewal and differentiation. *Cell Stem Cell* **22**, 221–234.e8 (2018).
69. Bonaguidi, M. A. et al. In vivo clonal analysis reveals self-renewing and multipotent adult neural stem cell characteristics. *Cell* **145**, 1142–1155 (2011).
70. Liu, L. et al. Exercise reprograms the inflammatory landscape of multiple stem cell compartments during mammalian aging. *Cell Stem Cell* **30**, 689–705.e4 (2023).
71. Schmidt, C. A., Fisher-Wellman, K. H. & Neufer, P. D. From OCR and ECAR to energy: perspectives on the design and interpretation of bioenergetics studies. *J. Biol. Chem.* **297**, 101140 (2021).
72. Knobloch, M. et al. A fatty acid oxidation-dependent metabolic shift regulates adult neural stem cell activity. *Cell Rep.* **20**, 2144–2155 (2017).
73. Delgado, A. C. et al. Release of stem cells from quiescence reveals gliogenic domains in the adult mouse brain. *Science* **372**, 1205–1209 (2021).
74. Merkle, F. T., Mirzadeh, Z. & Alvarez-Buylla, A. Mosaic organization of neural stem cells in the adult brain. *Science* **317**, 381–384 (2007).
75. Poisa-Beiro, L. et al. Glycogen accumulation, central carbon metabolism, and aging of hematopoietic stem and progenitor cells. *Sci. Rep.* **10**, 11597 (2020).
76. Pala, F. et al. Distinct metabolic states govern skeletal muscle stem cell fates during prenatal and postnatal myogenesis. *J. Cell Sci.* **131**, jcs212977 (2018).
77. Lin, S. J. et al. Calorie restriction extends *Saccharomyces cerevisiae* lifespan by increasing respiration. *Nature* **418**, 344–348 (2002).
78. Marcellino, B. K., Ekasumara, N. & Mobbs, C. V. Dietary restriction and glycolytic inhibition reduce proteotoxicity and extend lifespan via NHR-49. *Curr. Neurobiol.* **9**, 1–7 (2018).
79. Schulz, T. J. et al. Glucose restriction extends *Caenorhabditis elegans* life span by inducing mitochondrial respiration and increasing oxidative stress. *Cell Metab.* **6**, 280–293 (2007).
80. Lee, S. J., Murphy, C. T. & Kenyon, C. Glucose shortens the life span of *C. elegans* by downregulating DAF-16/FOXO activity and aquaporin gene expression. *Cell Metab.* **10**, 379–391 (2009).
81. Schlotterer, A. et al. *C. elegans* as model for the study of high glucose-mediated life span reduction. *Diabetes* **58**, 2450–2456 (2009).
82. Frolich, L. et al. Brain insulin and insulin receptors in aging and sporadic Alzheimer's disease. *J. Neural Transm.* **105**, 423–438 (1998).
83. Davidsohn, N. et al. A single combination gene therapy treats multiple age-related diseases. *Proc. Natl Acad. Sci. USA* **116**, 23505–23511 (2019).
84. Bernardes de Jesus, B. et al. Telomerase gene therapy in adult and old mice delays aging and increases longevity without increasing cancer. *EMBO Mol. Med.* **4**, 691–704 (2012).

Methods

Laboratory animals

Cas9-expressing mice (Cas9 mice) were obtained from the Jackson Laboratory (https://www.jax.org/strain/024858). These mice (background C57BL/6N) constitutively express the Cas9 endonuclease and an eGFP reporter under the control of a CAG promoter knocked into the *Rosa26* locus[49]. All screens in this study were performed with the Cas9 mice, including all NSC primary cultures and all in vivo work. We maintained a colony of Cas9 mice ranging in ages up to 28 months at the Stanford Comparative Medicine Building and the Neuroscience-ChemH building vivarium. As a negative control for the in vivo screens, male C57BL/6 mice obtained from the National Institute on Aging Aged Rodent colony were used at 18–21 months old. These mice were habituated in the Stanford facility for at least 2 weeks before initiation of experiments. Mice were maintained under the care of the Veterinary Service Center at Stanford University under IACUC protocols 8661.

Primary cultures of NSCs from young and old brains and activation experiments

For all experiments involving primary culture of NSCs, we pooled SVZs from pairs of male and female Cas9 mice, either 3–4 months old (young) or 18–21 months old (old). To generate primary cultures of NSCs from young and old mice, we microdissected SVZs into a small drop of PIPES buffer (pH 7.4), minced them in a 10 cm tissue culture dish with about 100 chops of a scalpel blade and suspended the tissue in PIPES buffer before centrifugation for 5 min at 300*g*, at which point the excess PIPES buffer was poured out. The pellet of minced SVZs was then enzymatically dissociated (in 5 ml per 2 SVZs) with a mixture of HBSS (Corning, 21-021-CVR) with 1% penicillin–streptomycin–glutamine (Gibco, 10378-016), 1 U ml^{-1} Dispase II (StemCell Technologies, 07913), 2.5 U ml^{-1} papain (Worthington Biochemical, LS003126) and 250 U ml^{-1} DNAse I (D4527, Sigma-Aldrich), vortexed briefly and incubated at 37 °C for 40 min on a rotator. The samples were then centrifuged at 300*g* for 5 min at room temperature and resuspended in Neurobasal A medium (Gibco, 10888-022) with 1% penicillin–streptomycin–glutamine (Gibco, 10378-016) and 2% B27 minus vitamin A (Gibco, 12587-010) and triturated about 20 times, centrifuged and resuspended in complete 'aNSC medium', comprising Neurobasal A (Gibco, 10888-022) supplemented with 2% B27 minus vitamin A (Gibco, 12587-010), 1% penicillin–streptomycin–glutamine (Gibco, 10378-016), 20 ng ml^{-1} EGF (Peprotech, AF-100-15) and 20 ng ml^{-1} bFGF (Peprotech, 100-18B) and placed in a humidified incubator at 37 °C and 5% CO_2. After 3–4 days, neurospheres emerged in the medium and were passaged by dissociation with 1 ml Accutase (StemCell Technologies, 07920) for 5 min at 37 °C, washed once with PBS and resuspended in aNSC medium. Neurosphere cultures were maintained with passaging every 2–3 days, and all experiments were performed in cultures of fewer than 10 passages. Details on passage numbers are provided in experimental sections below. For cultures of qNSCs, the aNSC culture medium was changed to remove EGF and to add BMP4 (50 ng ml^{-1}) (Peprotech, 315-27). The Complete 'qNSC medium' comprised Neurobasal-A (Gibco, 10888-022) supplemented with 2% B27 minus vitamin A (Gibco, 12587-010), 1× penicillin–streptomycin–glutamine (Gibco, 10378-016), 50 ng ml^{-1} BMP4 (BioLegend, 94073) and 20 ng ml^{-1} bFGF (Peprotech, 100-18B). To induce quiescence, tissue culture plates were pre-treated with PBS (Fisher Scientific, MT21040cv) containing 50 ng ml^{-1} poly-D-lysine (PDL; Sigma-Aldrich, P6407) for 1 h and then washed 3 times with PBS before plating cells on plates in qNSC medium. The density of cells plated is important for induction of quiescence and the ability of qNSCs to reactivate, especially in the context of lentiviral infection. In optimizing the qNSC activation protocol, we observed that qNSCs seeded at the following densities were best for quiescence and activation experiments: 2×10^7 cells for a 15 cm plate; 1×10^6 cells per well for a 6-well plate; 2×10^5 cells per well for a 24-well plate; and 1×10^5 cells per well for a 96-well plate. For activation of qNSC cultures, cells were washed once with PBS, and then aNSC medium was added to the plate and refreshed every 2 days. For plating, cells were manually counted with a haemocytometer or using a Countess II FL Automated Cell Counter (Life Technologies, AMQAF1000). NSC primary cultures were tested quarterly for the presence of mycoplasma and tested negative.

Tissue culture plastics

We found that primary cultures of NSCs were sensitive to the tissue culture plastic products used. Specifically, passaging NSCs in conical tubes manufactured by Genesee (15 ml conical tubes, 28-103) resulted in death of the NSC cultures within 1 week of brief exposure to the plastic during passaging. Plastics from the following manufacturers were assessed to be suitable for NSC growth both in detached and adherent conditions: Thermo Fisher 15/50 ml Falcon tubes (14-959-53A/14-432-22), 15 cm, 10 cm, 6-well, 12-well, 24-well and 96-well Falcon tissue culture dishes (353025, 08772E, 08-772-1B, 08-772-29, 08-772-1, 087722c, respectively).

Lentivirus production

Genome-wide virus library preparation. For lentiviral production, we used human embryonic kidney 293T cells. 293T cells were from the American Type Culture Collection (they were not authenticated). They were tested for the presence of mycoplasma in a quarterly manner and tested negative. 293T cells were seeded in DMEM + 10% FBS (Gibco 10099141) + 1× penicillin–streptomycin–glutamine (Gibco, 10378-016) at a density of 2×10^7 cells in 15 cm plates. One day later, 293T medium was replaced with 18 ml fresh medium and the cells were transfected using the polyethylenimine (PEI) (1 mg ml^{-1}, Polysciences, 23966-2) transfection method, mixing plasmids as follows: 2.27 µg each of third-generation lentivirus packaging vectors pMDLg, pRSV and pVSVG (obtained from the laboratory of M. Bassik), along with 45 µg of the pooled sgRNA genome-wide plasmid library (https://www.addgene.org/pooled-library/bassik-mouse-crispr-knockout/). The sgRNA library targets around 23,000 protein-coding genes in the genome, with 10 unique sgRNAs per gene, and15,000 control sgRNAs (about 245,000 sgRNAs in total)[29]. The sgRNA plasmid library, consisting of 20 sublibraries, was mixed proportionally to the number of sgRNAs in each library. One day after PEI transfection, the medium was changed to 18 ml of Neurobasal A + 1× penicillin–streptomycin–glutamine (Gibco, 10378-016). After 1 day, the viral containing supernatant was collected on ice and stored at 4 °C. Fresh medium was added to the 293T cells and collected again after 24 h and again at 48 h (a total of 3 collections of 18 ml of virus supernatant). All 3 supernatants were combined, filtered through a 0.45 µm filter (Stericup, EMD Millipore, S2HVU02RE) and frozen at −80 °C in 10 ml aliquots in 15 ml conical tubes. For plasmid library re-amplifications, we electroporated 1 µl of 25 ng $µl^{-1}$ of each library into 50 µl bacteria (Lucigen, 60242-2), with 1.8 kV, 600 Ω and 10 µF in a 0.1 cm cuvette (Gene Pulser Xcell, Bio-Rad, 1652662). After electroporation, we allowed bacteria to recover in Lucigen recovery medium for 2 h in 15 ml conical tubes, shaking at 37 °C. We plated 1 µl of the transformation onto a LB + carbenicillin (100 µg ml^{-1}, Sigma-Aldrich, C9231-1G) agar plate to confirm transformation efficiency, and the remainder of the recovery suspension was placed into 0.5 litre LB + carbenicillin (100 µg ml^{-1}) liquid medium in a 2 litre flask for 16 h of shaking at 37 °C, and DNA was purified using a Maxiprep kit (Thermo Fisher Scientific, FERK0492) according to the manufacturer's protocol.

sgRNA sublibrary design. We designed five sublibraries of sgRNAs to test gene hits from the in vitro screens in the brain in vivo (Figs. 1 and 2). Our selection criteria were as follows. For the top 10 gene list, we selected all significantly enriched genes (FDR < 0.1) from the first 2 in vitro genome-wide screens, selecting any gene that was significant in both screens 1 and 2, at any time point, day 4 or day 14 (for example, a screen 1 day 4 hit and an overlapping screen 2 day 14 hit would be added

to the list). With that list, we ranked the genes based on the CasTLE gene score average from both screens and both time points (that is, average of all: screen 1 day 4 or day 14, screen 2 day 4 or day 14). This library was selected based on the first two in vitro genome-wide screens only, because at the time of library design, only the first two in vitro screens had been completed. Similarly, the 'depleted' gene list was also selected based on the first two screens. We selected all significantly depleted genes (FDR < 0.1) from the first 2 in vitro genome-wide screens, selecting any gene that was significant in both screens 1 and 2, at any time point, day 4 or day 14 (for example, a screen 1 day 4 hit and an overlapping screen 2 day 14 hit would be added to the list). With that list, we then removed any gene that was significantly (FDR < 0.1) depleted in qNSCs of screen 1 or 2 of any age. The final list was then selected by removing unannotated genes (for example, GM3264 and GM3164) and focusing on genes with associated publications. For the 'glucose uptake/human disease' list, we selected genes that were significantly (FDR < 0.1) enriched in 2 out of 3 in vitro genome-wide screens, at day 4 or day 14 (for example, a screen 1 day 4 hit and an overlapping screen 2 day 14 hit would be added to the list). The list of enriched genes was analysed by GO term analysis (see the section 'Computational analysis of CRISPR screens'). From the GO Molecular Function (2018) database, the D-glucose transmembrane transporter activity (GO:0055056) and sugar:proton symporter activity (GO:0005351) terms were both in the top 10, with genes *Slc2a4*, *Slc2a12* and *Slc45a4*. The other genes in the 'glucose uptake/human disease' list were selected based on one of two criteria: (1) genes implicated in human disease: *Snrpb2* (Alzheimer's disease)[85], *Sorl1* (Alzheimer's disease)[86] and *C1qtnf5* (human ageing)[87]; or (2) genes that are significantly ($P < 0.05$) upregulated in qNSCs in old mice: *Slit2* (refs. 25,88), *Ier2* (ref. 25), *Cdkn1a*[25,88] and *Ecscr*[25]. For the 'cytoplasmic ribonucleoprotein granules' library, in the GO term analysis of gene knockouts that boosted old NSC activation, the terms P-body (GO:0000932), cytoplasmic ribonucleoprotein granule (GO:0036464), ribonucleoprotein granule (GO:0035770) and cytoplasmic stress granule (GO:0010494) all came up in the list, although most were not significant. From this, we proposed that cytoplasmic granule structures could impede old NSC activation. We took the entire GO term cytoplasmic ribonucleoprotein granule (GO:0036464) and selected gene knockouts that had the greatest difference in effect between young and old NSC screens. Many of these genes did not demonstrate any significant effect in our in vitro screens, other than *Dis3l2*, *Edc3* and *Mbnl1*, which all significantly boosted old NSC activation in at least two out of three screens. The final list of genes was the 'published NSC regulators' list, which we chose based on searching the literature for genes that had previously been implicated in regulation of NSC function and behaviour. We did not select based on functional effect prediction.

sgRNA plasmid sublibrary cloning for in vivo screens. The sgRNA expressing plasmid MCB320 (https://www.addgene.org/89359/) was digested with the BlpI and BstXI restriction enzymes, the band was gel-extracted and purified and used for a pooled ligation reaction. We selected five sgRNAs from each gene of interest, based on the five out of ten sgRNAs most enriched or depleted in our genome-wide in vitro screen. For the forward oligonucleotide of each sgRNA sequence, we added the following sequences: 5′-ttgg and 3′-gtttaagagc. For the reverse complement oligonucleotide of each sgRNA sequence, we took the reverse complement of the sgRNA sequence and added 5′-ttagctcttaaac and 3′-ccaacaag. To clone a pool of 10 genes, we selected the 50 sgRNAs pairs targeting the 10 genes and annealed the sgRNA pairs in separate annealing reactions in a 100 µl of IDT duplex buffer (11-05-01-12) with 1 µM forward and reverse oligonucleotides. We incubated the oligonucleotide pairs at 95 °C for 5 min and then allowed the oligonucleotides to gradually anneal at room temperature. We mixed all 50 annealed oligonucleotide pairs into one pool, diluted it 1:20 in IDT duplex buffer and then used 1 µl of annealed oligonucleotide pool in a ligation reaction with 500 ng of digested MCB320 backbone. We used 1.5 µl of the ligation mix and electroporated 30 µl competent bacteria (Lucigen, 60242-2) with 1.8 kV, 600 Ω and 10 µF in a 0.1 cm cuvette (Gene Pulser Xcell, Bio-Rad, 1652662). We plated the entire recovered transformed bacteria on a 10 cm LB + ampicillin (100 µg ml^{-1}, Sigma-Aldrich, A9518-100G) plate, allowed overnight recovery, and the next day added 5 ml LB to the bacterial lawn and scraped it with a sterile silicon scraper. The resuspended bacterial mix was transferred to a clean collection tube, the plate was again rinsed with an additional 5 ml LB and transferred to same tube for overnight growth in 500 ml LB + ampicillin (100 µg ml^{-1}) for Maxiprep (Thermo Fisher Scientific, FERK0492) according to the manufacturer's protocol. For library re-amplification, we performed the same transformation and amplification procedure.

Concentration of virus for in vivo and in vitro subscreens. For in vivo and in vitro subscreens, we generated virus the same way as our genome-wide virus libraries but with modifications. We plated four 15 cm plates of 293T cells for a total of 200 ml of collected virus after 3 days of collecting at 4 °C, but rather than directly freezing the virus, we performed ultracentrifugation to concentrate the virus. For ultracentrifugation, we sterilized 30 ml ultraclear tubes (Beckman Coulter 344058) under UV (TC room biosafety cabinet) for 15 min. We then put the tubes on ice, allowed 15 min to cool and then added 30 ml of virus and centrifuged at 16,500 r.p.m. for 1 h at 4 °C. We carefully decanted the supernatant using serological pipettes, leaving 1 ml medium in the bottom of the tube, adding 30 ml more virus-containing medium and centrifuging again. We repeated the decanting, refilling and centrifugation of the same tube, concentrating a total of 180 ml of virus supernatant into a single tube. After the last ultracentrifugation, we removed most of the supernatant with a serological pipette, and the last 1 ml with a P1000 pipet tip from the side of the tilted tube, so as not to disturb the viral pellet. The viral pellet was usually visible in centre of all of the tubes. We resuspend in 60 µl ice-cold PBS (1/3,000th original volume) by pipetting up and down about 60 times, being careful not to produce air bubbles. The concentrated resuspended virus was then aliquoted into PCR strip tubes in 5 µl aliquots and placed onto dry ice. After 15 min, the virus was transferred to −80 °C for storage. For experiments, virus was thawed on ice and injected into the brain or added to cell culture within 30 min of thawing. We assessed virus infectivity of each batch by performing serial dilution (3 µl, 1 µl, 0.5 µl) infections of 2×10^5 293T cells in 24-well culture plates for 16 h of infection and then performing FACS analysis 48 h later to detect the per cent of cells expressing the mCherry reporter. For each experiment, we normalized virus infectivity (viral titre) across treatments by adjusting the concentrations of virus added in PBS.

Genome-wide knockout screens in primary cultures of NSCs

For each genome-wide screen, primary cultures of NSCs derived from a pool of three male and three female Cas9 mice were used for each independent biological replicate. In total, three independent genome-wide screens, each performed with independent young and old NSC pooled from six mice, were conducted. For each independent screen, young and old NSC cultures were processed in parallel at each stage of sample processing. The young and old NSC culture passage numbers were kept the same and at the start of screen were as follows: screen 1, passage 8; screen 2, passage 7; screen 3, passage 12. To measure the growth rates of young and old cells at each passage, we counted cells using a Countess 3 cell counter (Thermo Fisher, A50298). The young and old cells showed comparable growth rates (Extended Data Fig. 1c). To expand the NSCs up to 1.4×10^9 cells (the equivalent of 140 15 cm plates) required for each biological replicate, 1×10^7 NSCs were passaged and expanded into 15 cm plates every 2–3 days, with feedings every 2 days (alternating between doubling the medium (with 2× growth factor aNSC medium) or complete medium exchange). For each screen, 70 plates of 2×10^7 qNSCs were seeded at day 0 (see below for library coverage

calculations). After 4 days in qNSC medium, the cells were incubated with the genome-wide sgRNA lentivirus library (see above). For this, the sgRNA lentivirus library was freshly thawed at room temperature and diluted 1:5 in Neurobasal medium and then B27 and growth factors were added to make it qNSC medium, and 18 ml of this mix was added to plates for 16 h of overnight infection. The virus dilution added was based on viral titration experiments determined to achieve about 30% culture infection of cells to ensure each cell only received a single sgRNA. Therefore, infecting the starting 1.4×10^9 cells at 30% infection would result in 4.2×10^8 infected cells, giving us a coverage of about 1,700 cells per sgRNA (around 243,000 total sgRNAs). Note that these numbers represent the starting library coverage, but the cells do expand over the course of activation; therefore, the final cell numbers at end of experiment are orders of magnitude larger. The infected cells were then left in qNSC medium for an additional 5 days before transition to aNSC medium for activation. After 4 days of activation, the cells were dissociated using Accutase (Stem Cell Technologies, 07920) for 15–30 min at 37 °C (until most cells rounded up) and gently scraped with silicone cell scrapers (Fisher Scientific, 07-200-364) and split into 2 groups: 55 plates of NSCs were processed for the day 4 Ki67 FACS sorting (see below), and the other 15 plates of cells were placed into aNSC culture for 10 days of further expansion as neurospheres (day 14 timepoint). The day 4 FACS-sorted young and old cells were sorted to have equal numbers of $Ki67^+$ cells from both ages for each screen for downstream analysis. See the section 'Intracellular FACS' below for day 4 FACS protocol. The final number of sorted cells for each age in each screen was as follows: screen 1 had 2.2×10^7 sorted $Ki67^+$ cells; screen 2 had 1.41×10^7 $Ki67^+$ cells; and screen 3 had 1×10^8 $Ki67^+$ cells. After sorting, the methanol-fixed cells were centrifuged at 700*g* for 5 min, the supernatant FACS buffer was decanted and the cell pellets were frozen at −80 °C until genomic DNA extraction. To extract genomic DNA of sorted and methanol-fixed cells, the cell pellets were defrosted at room temperature and then processed by resuspending in 5 ml of TE 1% SDS (Thermo Fisher Scientific, 15525017) and incubated at 65 °C for 16 h. The cell suspension was then treated with 50 µl proteinase K (Fisher Scientific, 25-530-049)(20 mg ml^{-1}) for 2 h at 37 °C. Samples were processed for genomic DNA extraction using Zymo Research ChIP DNA clean and concentrator (Zymo, D5205) according to manufacturer's protocol. The day 14 expanding neurospheres were immediately centrifuged at 300*g* for 5 min and then processed for genomic DNA extraction with a Qiagen QiaAmp DNA Blood Maxi kit (51194), adding 5×10^7 cells per column and according to the manufacturer's protocol.

sgRNA PCR amplification and sequencing

After genomic DNA isolation, sgRNA was amplified from the genome in two successive, nested PCR reactions. For the nested PCR reactions, we used either Herculase II Fusion polymerase (Agilent, 600679) for screen 1 or Q5 DNA polymerase (Fisher Scientific, M0491L) for screens 2 and 3, and Q5 DNA polymerase for in vivo screens, according to the manufacturer's protocol. In optimizing this PCR reaction, we found that Herculase II polymerase was outperformed by Q5 polymerase, with Q5 polymerase requiring fewer PCR cycles to obtain more amplicon product, which is why we switched to Q5 DNA polymerase. We used 5 µg genomic DNA in 50 µl reactions to run on a thermocycler. For the first PCR, we used primers MCB1562 (aggcttggatttctataacttcgtatagcatacattatac) and MCB1563 (acatgcatggcggtaatacggttatc) (1 µM final concentration), with PCR cycles as follows: 98 °C for 2 min, 19 cycles of (98 °C for 30 s, 59.1 °C for 30 s, 72 °C for 45 s), followed by 72 °C for 3 min. We pooled all the PCR 1 cycle products and then used 5 µl of the pool in a second PCR reaction (PCR 2) with the same conditions but using different primers: MCB1439 (caagcagaagacggcatacgagatgcacaaaaggaaactcaccct) and a barcoded primer (aatgatacggcgaccaccgagatctacacGATCGGAAGAGCACACGTCTGAACTCCAGTCACXXXXXXCGACTCGGTGCCACTTTTTC, where XXXXXX is the 6-digit barcode for high-throughput sequencing sample identification). The second PCR reaction was run for either 30 cycles (in vitro screen 1 and in vivo screens) or 18 cycles (in vitro screens 2 and 3). The resulting PCR products were all resolved on a 1.5% DNA agarose gel. The 272 bp band was extracted (Qiaquick Gel extractions kit, 28706), eluted in 10 µl ultrapure water (Invitrogen, 10977023) and assessed on a bioanalyzer (Agilent, Bioanalyzer 2100). Final libraries were combined into a pool at equal concentrations for sequencing on an Illumina Novaseq S4 system (by Novogene for the genome-wide in vitro screen) or on an Illumina MiSeq system (by the Stanford Genomics Facility for in vivo screens), sequencing to a depth of about 1×10^7 or 5×10^5 reads per sample for in vitro and in vivo screens, respectively.

Computational analysis of CRISPR–Cas9 screens

For both the in vitro and in vivo screens, our analyses were performed using the CasTLE pipeline[28]. All of the source scripts can be found at Bitbucket (https://bitbucket.org/dmorgens/castle/downloads/). In brief, for each screen, the raw screen fastq files were aligned to the sgRNA library sequence (mm-Cas9-10 or one of a custom 10 gene library + control sgRNAs) to make count files using the makeCounts script. The count files were then analysed using the analyzeCounts CasTLE script, comparing each screen timepoint to the starting plasmid sgRNA library count file (in vitro screens) or the sequenced 24-h SVZ count file (in vivo screens), which we sequenced in parallel with screen libraries. We then calculated *P* values for all genes in each screen by running 100,000 (in vitro screens) or 10,000 (in vivo screens) permutations with the addPermutations CasTLE script. For each genome-wide screen, we corrected for multiple hypotheses on the around 23,000 gene associated *P* values using the Python Statsmodel module, with the Benjamini–Hochberg method, and classified genes as significant using a FDR < 0.1 cut-off. For the in vivo screens, we classified genes as hits if their CasTLE computed 95% confidence interval did not contain 0. The library diversity of each sample was displayed using the plotDist CasTLE script. The screen results and individual gene sgRNA enrichment plots were visualized using the plotVolcano and plotGene scripts, respectively. We note that in in vivo screens, there was a bimodal distribution of control sgRNAs, which is most likely due to the fact that a control sgRNA infected a NSC that was, at the time, highly actively proliferating and that will naturally enrich in the olfactory bulb.

Generation of gene lists for the genome-wide screens

To generate the final gene lists for the genome-wide screens, we used all genes that were significant (FDR < 0.1) in 2 or more independent screens (screens 1 and 2, 2 and 3, or 1 and 3), at any time point (day 4 or day 14; for example, a screen 1 day 4 hit and an overlapping screen 2 day 14 hit, would be added to the list). For PCA, we used the Python sklearn.decomposition.PCA module with CasTLE-computed gene scores as input (Fig. 1d and Extended Data Fig. 1g–i). We performed gene set enrichment analysis by inputting gene lists into the EnrichR online portal (https://maayanlab.cloud/Enrichr/)[89,90], and then focusing on the 'Ontologies' tab with GO Biological Process (2018), Molecular function (2018) and Cellular components (2018), sorting the terms based on *P* value, which is computed by EnrichR using the Fisher exact test.

Assessment of potential outliers in the genome-wide screens

To test for potential outliers, we compared CasTLE scores for all genes in the genome-wide screen between each replicate at day 14 for the young NSC screens (Extended Data Fig. 1d–f). Correlations between replicates were calculated using Spearman's correlation test. We also examined the principal component (PC) loadings of day 14 young and old in vitro genome-wide screens (PC1 and PC2) and day 4 young and old in vitro genome-wide screens (PC3 and PC4). PC loadings were extracted using the Python sklearn.decomposition.PCA module. We performed gene set enrichment analysis by inputting the top 50 gene knockouts contributing to the PC into EnrichR online portal (https://maayanlab.cloud/Enrichr/)[89,90], and then focusing on the 'Ontologies'

tab with GO Biological Process (2018), Molecular function (2018) and Cellular components (2018), sorting the terms based on *P* value, which is computed by EnrichR using the Fisher exact test. The PC loadings and the GO terms are included in Supplementary Table 4. The GO terms of the genes that contribute to the replicate young 1 at day 14 not clustering with the other young replicates are enriched for cytosolic proteasome complex (GO:0031597) and proteasome-activating ATPase activity (GO:0036402). As mentioned above in the section 'Generation of gene lists for the genome-wide screens', we chose hits from the screen that were significant in two or three replicates to avoid having one of the screens skew the data. We also investigated the loading of all PCs for both day 4 and day 14 and performed GO term analysis on the genes underlying all PCs (Supplementary Table 4). Genes and GO terms underlying the technical variance for day 4 samples (PC1, PC2 and PC4) are involved in cell division, proteostasis and transcription/translation. Thus, one possible source of variance in this in vitro NSC system could be due to lentiviral infection (affecting cell survival/cell proliferation) or bottlenecking during passaging.

Comparison with published screens and databases

We tested whether the genes significantly depleted at the day 14 timepoint overlapped with a list of common essential genes. We generated a list of day 14 significantly (FDR < 0.1) depleted genes in both the young and old screens (Supplementary Table 1). We identified the overlap between significantly depleted genes in the NSC screens with the Core Essential Genes 2 list[91] and the Online GEne Essentiality database (https://v3.ogee.info/#/home)[92] (Extended Data Fig. 1l,m). *P* values were calculated using a Fisher's exact test. There was a small but significant overlap between the known essential gene lists and the significantly depleted NSC gene list. Thus, these in vitro genome-wide screens captured essential genes that are shared with published datasets but also captured unique genes for which knockout affected cell survival or activation in NSCs.

Intracellular FACS for Ki67

For the genome-wide screen and for other qNSC activation experiments, we FACS-isolated proliferative cells ($Ki67^+$) as follows. Cells were dissociated with Accutase (StemCell Technologies, 07920) for 5 min, collected into conical tubes and centrifuged at 300*g* for 5 min. Cells were resuspended in PBS at 5×10^7 cells in 1 ml (or 1×10^5 cell in 100 µl), and then 9 ml (or 900 µl) ice-cold 100% methanol was added and cells were agitated for 15 min at 4 °C. Cells were then centrifuged at 500*g* for 5 min and resuspended for a wash in 3 ml PBS and centrifuged again at 500*g* for 5 min. Cells were then resuspended in 3.5 ml staining solution: Ki67-APC (eBioscience, 17-5698-82) 1:300 in PBS, 2% FBS (Gibco, 10099141) at 4 °C. Samples were agitated for 30 min at room temperature in the dark, and then 10 ml PBS was added before centrifugation at 700*g* for 5 min. Samples were then resuspended (25 ml per 5×10^7 cells) in FACS buffer: PBS, 2% FBS, DAPI (Fisher Scientific, 62248, 1 mg ml^{-1}) 1:5,000. Each sample was filtered with FACS-strainer cap tubes (Fisher, 08-771-23), immediately before FACS sorting. Cells were sorted on an Aria BD FACS Aria with a 100 µm nozzle at 13 p.s.i., with BD FACSDiva software (v.8.0.1), and FlowJo (v.10) software was used for data analysis.

Assessment of NSC activation for in vitro subscreen and glucose intervention

For testing the top 10 gene library (in vitro subscreen) (Fig. 1e) and glucose intervention (Fig. 4i), we performed qNSC activation experiments in a 24-well or 96-well format. We seeded 2×10^5 cells in a 24-well format or 1×10^5 cells in a 96-well format. After 4 days in qNSC medium, with medium changes every 2 days, concentrated virus was then added to the cells. We added 3 µl equal titre virus (see the section 'Concentration of virus for in vivo and in vitro subscreens') to each 24-well containing 500 µl qNSC medium, or 0.1 µl virus to 100 µl in each 96-well experiment. We left the virus in medium with cells for 16 h, and then refreshed the medium. At 5–6 days after infection, the cells were washed 1× in PBS and then either transitioned to aNSC medium for activation (Fig. 1e) or incubated with qNSC medium with or without glucose for 2 days and then transitioned to aNSC medium for activation (Fig. 4i). aNSC medium was exchanged once after 48 h and Ki67 intracellular FACS was performed at day 4 after infection (see the section 'Intracellular FACS' above). Even though overall activation was decreased in lentivirally infected cells compared with non-infected cells, the difference in activation between old and young NSCs was preserved.

Assessment of the impact of individual gene knockout on NSC activation

To test the impact of individual gene knockouts on NSC activation (Fig. 1j), we used 8 independent NSC cultures from old (18–21 months old) mice, each culture being a mix of 1 male and 1 female mouse. We infected these NSC cultures with purified lentiviruses expressing five sgRNAs per gene. We evaluated the top 10 genes (screens 1 and 2) (Supplementary Table 3). To assess the effect of each individual gene knockout on NSC activation, we seeded 3×10^5 NSCs in a 24-well format. After 4 days in qNSC medium, with medium changes every 2 days, qNSCs were incubated with fresh lentiviruses with equal titre. Lentiviruses were generated as described in the section 'Lentivirus production' using 293T cells. For these experiments, lentiviruses expressing sgRNAs to individual genes were collected by incubating 293T cells directly in qNSC medium. The supernatants were collected and their titres were tested, using serial dilutions to achieve a similar 50–70% range of infection of 293T cells. Supernatants were added to the qNSC wells for 16 h, and then the medium was changed to qNSC medium. Six days after infection, the cells were washed 1× in PBS and then transitioned to aNSC medium for activation. aNSC medium was exchanged once after 48 h and then Ki67 intracellular FACS was performed at day 3 after infection (see the section 'Intracellular FACS' above).

Validation of individual knockout efficiency

We validated the knockout efficiency for seven individual genes in qNSC cultures in two independent experiments:

For experiment 1, young and old NSCs were seeded in a 24-well PDL pre-coated plate at a density of $2–3 \times 10^5$ cells per well and incubated in qNSC medium. After 4 days with medium changes every 2 days, qNSCs were infected with lentiviruses expressing sgRNAs targeting each gene (5 sgRNAs per gene) as described in the section 'Assessment of the impact of individual gene knockout on NSC activation' (see Source Data Extended Data Fig. 1n for sgRNA sequences). Six days after infection, cells were washed with PBS then lysed directly with DirectPCR Lysis reagent (Viagen Biotech, 102-T) with 1% Proteinase K (Fisher Scientific, 25-530-049) for 10 min at room temperature. The supernatant was pipetted repeatedly, then transferred to PCR strip tubes and incubated at 65 °C for 25 min, and then 95 °C for 15 min in a thermocycler. We amplified genomic DNA with primer pairs surrounding the sgRNA-editing sites (see Source Data Extended Data Fig. 1n for amplification primers), using Q5 polymerase (Fisher Scientific, M0491L) and the following program: 30 s of annealing step at 55 °C and 1 min of extending step at 72 °C for 40 cycles total.

For experiment 2, we cloned 5 sgRNAs for each individual gene, using the same methodology as described in the section 'sgRNA plasmid sublibrary cloning for in vivo screens' above. For lentiviral production, 293T cells were seeded in DMEM + 10% FBS (Gibco 10099141) + 1× penicillin–streptomycin–glutamine (Gibco, 10378-016) at a density of 13×10^6 cells in 15 cm plates. One day later, 293T medium was replaced with 18 ml fresh medium and the cells were transfected using the PEI (1 mg ml^{-1}, Polysciences, 23966-2) transfection method. The individual gene library (25.5 µg) was transfected together with the lentiviral packaging plasmids psPAX2 (32.12 µg) and pCMV-VSV-G (9.44 µg) per 15 cm plate. psPAX2 was a gift from D. Trono (Addgene, plasmid 12260; http://n2t.net/addgene:12260; RRID:Addgene_12260). pCMV-VSV-G

was a gift from B. Weinberg (Addgene, plasmid 8454; http://n2t.net/addgene:8454; RRID:Addgene_8454). One day (20–24 h) after transfection, the medium was changed to Neurobasal A with penicillin–streptomycin–glutamine. After another 20–24 h, lentivirus containing supernatant was collected and stored at 4 °C and fresh medium was added to the 293T cells for another collection after 24 h. Both supernatants were then combined, filtered through a 0.45 µm polyvinylidene fluoride filter (Millipore Sigma, SE1M003M00) and frozen at −80 °C in 5 ml aliquots. For lentiviral transduction, young qNSCs were plated onto 6-well PDL pre-coated plates at a density of 1.75×10^6 cells per well (for control lentivirus), 10 cm PDL pre-coated plates at the density of 1.0×10^7 cells per plate (for *Slc2a4*-targeting lentivirus) or 12-well PDL pre-coated plates at a density of 4.0×10^5 cells (for *Npb* and *B3galnt2* targeting lentivirus). NSCs were kept in qNSC medium for 4 days (with medium changes every other day) before transduction. After removing medium, viral supernatants (2 ml for 6-well plates, 10 ml for 10 cm plates and 1 ml for 12-well plates) were thawed at room temperature and mixed with 8% of B27 minus vitamin A, bFGF (80 ng ml^{-1}) and BMP4 (200 ng ml^{-1}). qNSCs were incubated with lentiviral medium for 24 h. After removing lentiviral medium after 24 h, a second lentiviral transduction was repeated the next day. After two consecutive transductions, qNSCs were washed once with Neurobasal A medium and then cells were kept in qNSC medium for 7 days to allow recovery and CRISPR editing. To select for a population of cells that was infected by the lentivirus, 1.0 µg ml^{-1} of puromycin (Sigma-Aldrich, P8833) was added to the cultures for 3 days, with medium changes every day. To assess knockout efficiency, we isolated genomic DNA as described above for experiment 1. We amplified genomic DNA with primer pairs roughly 150–250 bp upstream and 300–450 bp downstream of sgRNA editing site (see source data for list of primers) using GoTaq Green master mix (Promega, M7123) and the following amplification program: 30 s of annealing step at 55 °C and 1 min of extending step at 72 °C for 40 cycles total.

In both experiment 1 and experiment 2, PCR amplicons were Sanger sequenced using the respective forward primers (source data). We then analysed knockout efficiency using the DECODR (v.3.0) online tool (https://decodr.org/)[93]. Each sgRNA was analysed separately, and the editing efficiency is indicated in source data. Individual sgRNAs that had an editing efficiency with a r^2 value less than 0.6 from DECODR (v.3.0) are indicated as low confidence (LC) in source data and marked with a hash symbol in Extended Data Fig. 1n. Individual sgRNAs that were not detected by DECODR (v.3.0) in the Sanger sequencing trace are indicated as not detected (ND) in source data and not included as data points in Extended Data Fig. 1n. Finally, we note that the percentage of knockout per gene is probably also underestimated due to the fact that larger indels that span sgRNA cutting sites are not taken into account by DECODR.

In vivo gene knockout experiments

Stereotaxic surgeries were performed to inject virus into the lateral ventricle of mice. For these experiments, old Cas9 mice were used, except for one experiment for which old wild-type mice were used (see the section 'Laboratory animals'). Surgeries were performed on heating pads with isoflurane-induced anaesthesia, with a Kopf (Model 940) stereotaxic frame, World Precision Instruments (UMP3T-1) UltraMicroPump3, Hamilton 1710RN 100 µl syringe with 30 g Small Hub RN needle with a point 2 bevelled end. Injections were made at the following coordinates, relative to bregma: lateral 1 mm, anterior 0.3 mm and ventral depth 3 mm from the skull surface. After drilling the skull and inserting the needle into position, we waited 5 min before injecting the virus. We injected 3 µl of equal titre virus at a rate of 10 nl s^{-1}. We waited 7 min after injection before removing the needle and suturing the skin. Animals were administered a single dose of buprenorphine SR (0.5 mg kg^{-1}) for postoperative pain management and monitored for 1 week after surgery until full recovery. For labelling of proliferating NSC progeny, we injected animals intraperitoneally weekly with EdU (Thermo Fisher Scientific, A10044, 50 mg kg^{-1}, dissolved in sterile PBS), starting 1 week after surgery. We used both male and female mice for in vivo testing, always making a note of the sex for each experiment. We did not observe major differences in results between sexes, and plots include data from both sexes.

Influence of the anaesthetic. In our pilot experiments, we performed some surgeries with ketamine–xylazine anaesthesia instead of isoflurane for the relative ease of use, which we consider resulted in marked impairment of neurogenesis in both young and old animals when assessed in downstream screen analyses. In brief, we performed our in vivo screening as outlined above, but we could detect only very few sgRNAs in the olfactory bulb 5 weeks after injection when the mice had been anaesthetized with ketamine–xylazine. We interpreted the lack of sgRNA detection in the olfactory bulb as an indication that not many NSCs were able to activate and migrate to the olfactory bulb in those conditions. We repeated the experiments with ketamine–xylazine 2 times, in around 20 animals, always observing an impairment in sgRNA detection in the olfactory bulb after 5 weeks. When the same virus was injected into same age and background mice under isoflurane anaesthesia, we detected a greater diversity and abundance of sgRNAs in the olfactory bulb 5 weeks later. We therefore did not perform any surgeries presented in this article with ketamine–xylazine anaesthesia, but used isoflurane instead.

At the end point of in vivo experiments, mice were either killed for sequencing of sgRNAs in the brain (in vivo subscreens) or for immunofluorescence imaging (see the section 'In vivo immunofluorescence experiments') of the olfactory bulb and other brain regions (single gene knockout experiments). For sequencing sgRNAs in the brain, mice were killed either 1–2 days after injection or 5 weeks after injection and their brains were immediately removed and subdissected for genomic DNA extraction. We used a scalpel to cut off the olfactory bulbs and to cut an approximately 1 mm thin slice of the outer cortex as well as the outer cerebellum. We then subdissected out the SVZ niche. We took each tissue and minced it with around 100 cuts of a scalpel and proceeded to extract genomic DNA according to the manufacturer's protocol (Qiagen QIAamp DNA micro kit, 56304). The genomic DNA was then processed for sgRNA amplification and sequencing as outline in the section 'sgRNA PCR amplification and sequencing'.

Immunofluorescence staining of brain sections, image analysis and quantification

Brain sections in the olfactory bulb and SVZ. For immunofluorescence straining of brain sections, young and old anaesthetized mice were first subjected to intracardiac perfusion with 4 ml of heparin (Sigma Aldrich, H3149-50KU) and then 25 ml 4% paraformaldehyde (PFA) (Electron Microscopy Science, 15714) in PBS. Brains were then removed and further fixed for 16 h by submerging in 4% PFA at 4 °C. Brains were then washed 3 times in PBS and placed in a conical tube with a 30% sucrose (Sigma-Aldrich, S3929-1KG) in PBS solution for 2–3 days until sinking to bottom of conical tube. The brains were then embedded in optimal cutting temperature (OCT) compound (Electron Microscopy Sciences, 62550-12) for cryosectioning. Brain coronal sections were taken at 20 µm thickness (Leica, CM3050S). For assessing neurogenesis in the olfactory bulb, every tenth section was used. Thus, imaging was performed every 200 µm across the entire olfactory bulb. For assessing different cell types in the SVZ, we began taking sections at the most anterior part of the lateral ventricle, and every tenth section was used. Thus, imaging was performed every 200 µm across the SVZ.

Immunofluorescence staining of brain sections. For immunofluorescence staining, sections were brought to room temperature and then washed once with PBS and then permeabilized with ice-cold methanol and 0.1% Triton X-100 (Fisher Scientific, BP151) for 15 min. All samples

were stained at the same time. Slides were washed 3 times with PBS and then treated with ClickIt reagents (for EdU) or put straight into antibody blocking solution. For Click-It EdU staining (Thermo Fisher Scientific, C10337/C10639/C10634), we placed 50–70 µl of reaction cocktail from this kit onto the tissue and incubated in humidified chamber at room temperature for 30 min. Slides were then washed 3 times in PBS before blocking for antibodies. Slides were treated with 50–70 µl blocking solution (5% normal donkey serum (NDS, ImmunoReagents, SP-072-VX10), 1% BSA (Sigma-Aldrich, A1595-50ML), 8.5 ml PBS) in a humidified chamber at room temperature for 30 min. Blocking solution was replaced with antibody solution consisting of blocking solution with antibodies as follows: mCherry (Invitrogen, M11217, clone 16D7) 1:500, GFAP (Abcam, 53554) 1:500, GFP (Abcam, 13970) 1:500, GLUT4 (for in vivo staining R&D Systems, MAB1262, clone 1F8) 1:500, Ki67 (Invitrogen, 14-5698-082, clone SolA15) 1:500, STX4A (Santa Cruz Biotechnology, sc-101301, clone QQ-17) 1:500, GFP (Abcam, 13970) 1:500, mouse IgG (Santa Cruz SC-3877, lot: L1916) 1:500, NeuN (Millipore, MAB377 clone A60) 1:500, S100a6 (Abcam, ab181975, clone EPR13084-69) 1:500, Tuj1 (BioLegend, 802001) 1:500, Olig2 (R&D Systems, AF2418) 1:100, Sox10 (Abcam, Ab180862, clone EPR4007-104) 1:100, calretinin (Abcam, Ab244299) 1:500, Dcx (Cell Signaling Technology, 4604) 1:500. We tested two mCherry antibodies (Abcam, ab213511 clone EPR20579; Invitrogen, M11217 clone 16D7) and we found that Invitrogen, M11217 was better for immunostaining for brain sections. After primary staining in dark for 2 h in humidified chamber at room temperature or 16 h at 4 °C, slides were washed 3 times in PBS before staining with secondary antibodies. Secondary antibodies were diluted in blocking solution and consisted of Alexa 488/594/647 conjugated antibodies (Fisher Scientific, A21202, A21206, A21209, A21447, A31571, A31573) 1:500, and DAPI (1 mg ml^{-1}, Fisher Scientific 62248) 1:5,000. We added 50–70 µl of secondary antibody mix to cover the section and incubated in the dark for 2 h in a humidified chamber at room temperature or 16 h at 4 °C. Slides were then washed 3 times with PBS 0.2% Tween for 10 min, washed 3 times with PBS for 5 min and then mounted using ProLong Gold (20–40 µl, Thermo Fisher Scientific, P36931), dried for 2 h and sealed with nail polish. To allow for quantification of the immunofluorescence staining, we paid special attention to stain all the brain sections from different groups (for example, young and old) in the same way and at the same time.

Confocal imaging of immunofluorescence staining in brain sections. Images were captured using a Zeiss LSM 900 confocal microscope with a ×10, ×20 or ×63 objective, with Zen blue edition (v.3.0). The exposure and gain settings for each channel and antibody were set at the beginning of each imaging session and remained the same for all animals and treatments. We randomized the order in which we imaged the slides and we ensured that different treatments and age groups were all imaged in the same session on the same day. The imaging was not performed in a blinded manner. We did not select areas to image. We imaged and quantified serial sections. Confocal imaging was done every 200 µm across the entire olfactory bulb or SVZ region.

Image analysis and quantification of immunofluorescence staining in brain sections. For image analysis, we used the open-source software QuPath (https://qupath.github.io/)[94]. This approach allowed us to set the thresholds and quantification parameters on training images and then ran the same analysis across all sections, samples and treatments in an automated manner. Many cells (>100 cells per section in vivo) and many sections (>50 sections per age group in vivo) were counted in an unbiased manner using an automated pipeline (in QuPath).

Quantification of GLUT4 depletion efficiency in the SVZ niche by immunostaining in vivo. For quantifying GLUT4 depletion efficiency in the SVZ niche, we first annotated a polygonal line around the SVZ NSC niche, creating an analysis region about 5–20 cells deep from the ventricle wall. We then performed the 'analyse→cell detection' function, detecting cells in the image based on DAPI staining, using the program default settings, expanding the cell nuclei 5 µm in the 'cell parameters' section. We then trained two independent object classifications for GFAP$^+$ and mCherry$^+$ cells, adjusting the thresholds to detect positive cells that were apparent by eye. We combined the GFAP$^+$ and mCherry$^+$ objects into a single composite classifier and ran it on all annotated images and treatments. The results were output as annotation detections. The annotation detections were used to display the GLUT4 channel cell mean fluorescence intensity for GFAP$^+$mCherry$^+$ compared with GFAP$^+$mCherry$^-$ populations in the different treatments.

Quantification of newborn neurons in the olfactory bulb by immunostaining in vivo. For quantification of newborn neurons in the olfactory bulb, we first annotated a polygon line immediately beneath the olfactory bulb mitral cell layer to focus the analysis within the inner layers of the olfactory bulb, where newborn neurons arrive. We then performed the 'analyse→cell detection' function, detecting cells in the image based on DAPI staining, using the program default settings, expanding the cell nuclei 5 µm in the 'cell parameters' section. We then trained three independent object classifications for mCherry$^+$, EdU$^+$ and NeuN$^+$ cells, adjusting the thresholds to detect positive cells that were apparent by eye. We combined the mCherry, EdU and NeuN objects into a single composite classifier and ran it on all annotated images and treatments. The results were output as annotation measurements and annotation detections. The annotation measurements were used for graphs depicting the number of NeuN$^+$mCherry$^+$EdU$^+$/total EdU$^+$ cell numbers for each treatment, and the annotation detections were used to display the NeuN channel cell mean fluorescence intensity for EdU$^+$mCherry$^+$ populations in the different treatments.

Quantification of different cell numbers in the SVZ niche by immunostaining in vivo. For quantifying different cell numbers in the SVZ niche with *Slc2a4* sgRNA treatment compared with control, we first annotated a polygonal line around the SVZ NSC niche, creating an analysis region about 5–20 cells deep from the ventricle wall. We then performed the 'analyse→cell detection' function, detecting cells in the image based on DAPI staining, using the program default settings, expanding the cell nuclei 5 µm in the 'cell parameters' section. We then trained three independent object classifications for GFAP$^+$, Ki67$^+$ and S100a6$^+$ cells, adjusting the thresholds to detect positive cells that were apparent by eye. We combined the GFAP$^+$, Ki67$^+$ and s100a6$^+$ objects into a single composite classifier and ran it on all annotated images and treatments. The results were output as annotation measurements. The annotation measurements were used for graphs depicting the sgRNA treatment and impact on number of each cell type: qNSCs (GFAP$^+$S100a6$^+$Ki67$^-$), aNSCs (GFAP$^+$S100a6$^+$Ki67$^+$), neuroblasts (GFAP$^-$Ki67$^+$) and astrocytes (GFAP$^+$S100a6$^-$) for each condition.

Quantification of GLUT4 protein levels in different cell types of the SVZ niche by immunostaining in vivo. For quantification of GLUT4 fluorescence intensity in different cell types of young and old mice in vivo, we first annotated a polygonal line around the SVZ NSC niche, creating an analysis region about 5–20 cells deep from the ventricle wall. We then performed the 'analyse→cell detection' function, detecting cells in the image based on DAPI staining, using the program default settings, expanding the cell nuclei 5 µm in the 'cell parameters' section. We then trained two independent object classifications for Ki67$^+$ (or S100a6$^+$, for NSC specific labelling experiments) cells and GFAP$^+$ cells, adjusting the thresholds to detect positive cells that were apparent by eye. We combined the Ki67 (or S100a6) and GFAP objects into a single composite classifier and ran it on all annotated images and treatments. The results were output as annotation detections. The annotation detections were used to display the GLUT4 channel cell mean fluorescence intensity for GFAP$^+$Ki67$^+$ (aNSCs), GFAP$^+$Ki67$^-$ (qNSCs/astrocytes),

GFAP$^-$Ki67$^+$ (neuroblasts), GFAP$^-$Ki67$^-$ (other cells, including ependymal and microglia) or GFAP$^+$S100a6$^+$ (NSCs) populations across different aged mice. The GLUT4 antibody we used for immunostaining of brain sections (R&D Systems, MAB1262, clone 1F8) was validated in vivo by the *Slc2a4* knockout (see above).

For all experiments, the output numbers displayed on the graphs were derived from the average of all serial section images across a biological replicate (one mouse), biological sample values were then analysed for significance by two-tailed Mann–Whitney test.

Immunofluorescence staining of primary cell cultures of NSCs and quantification

Immunofluorescence staining of NSC cultures. For immunofluorescence staining of primary cell cultures of NSCs, we seeded 2.5×10^5 aNSCs or 2×10^5 qNSCs onto PDL (50 ng ml^{-1}, Sigma-Aldrich, P6407) pre-treated (30 min, followed by 3× PBS wash) coverslips in each well of a 24-well plate. The qNSCs were plated 7 days before fixation, the aNSCs were plated 24 h before fixation. For fixation, cells were washed once with PBS and then 500 µl of 4% PFA (Electron Microscopy Science, 15714) was added for 30 min of incubation at room temperature. Cells were washed 3 times with PBS and then permeabilized with 0.1% Triton X-100 (Fisher Scientific, BP151) in PBS for 15 min shaking at room temperature. Coverslips were washed twice with PBS and then processed for antibody staining. Coverslips were placed on a 45 µl drop of primary antibody solution consisting of 1% BSA in PBS with primary antibodies as follows: GLUT4 (Abcam, 33780) 1:500, Ki67 (Invitrogen, 14-5698-082) 1:500, STX4A (Santa Cruz Biotechnology, QQ-17) 1:500. After 1 h of incubation in the dark at room temperature, slides were washed 3 times in PBS shaking for 5 min at room temperature. Slides were then placed on 45 µl drop of secondary antibodies in 1% BSA in PBS consisting of Alexa 488/594/647 conjugated antibodies (Fisher Scientific, A21206, A21209, A31571) 1:500, and DAPI (1 mg ml^{-1}, Fisher Scientific 62248) 1:5,000. After 1 h of incubation at room temperature in the dark, slides were washed 3 times with PBS before mounting with ProLong Gold, dried for 2 h and sealed with nail polish. To allow quantification of immunofluorescence staining, we paid special attention to stain all coverslips in the same way and at the same time.

Confocal imaging of immunofluorescence staining in NSC cultures. Images were captured using a Zeiss LSM 900 confocal microscope with a ×10, ×20 or ×63X objective. The exposure and gain settings for each channel and antibody were set at the beginning of each imaging session and remained the same for all samples and treatments. We randomized the order in which we imaged the slides, and we ensured that different treatments and age groups were all imaged in the same session on the same day. The imaging was not done in a blinded manner. We did not select areas to image. We randomly selected ten areas of each coverslip to image. For image analysis, see the section 'Immunofluorescence image analysis'.

Image analysis and quantification of immunofluorescence staining in NSC cultures. For image analysis, we used the open-source software QuPath (v.0.2.3) (https://qupath.github.io/)[94]. This approach allowed us to set the thresholds and quantification parameters on training images and then ran the same analysis across all sections, samples and treatments in an automated manner. For the in vitro GLUT4 and STX4A quantifications, we selected the entire image as the analysis annotation. We then performed the 'analyse→cell detection' function, detecting cells in the image based on DAPI staining, using the program default settings, expanding the cell nuclei 5 µm in the 'cell parameters' section. The results were output as annotation detections. The annotation detections were used to display the GLUT4 and STX4A cell mean fluorescent intensity for each protein's channel in each cell culture type and age group. For all experiments, the output numbers from different images were averaged across a biological replicate (one NSC culture), biological sample values were then analysed for significance by two-tailed Mann–Whitney test. We note that the age-dependent increase in GLUT4 and STX4A proteins was not large in qNSC cultures. In addition, we were not able to detect significant changes in *Slc2a4* by RT–qPCR and western blotting in young and old qNSCs. This lack of detection is probably due to sensitivity issues: single-cell RNA sequencing and immunofluorescence staining are single-cell-based assays, which can be more sensitive than bulk assays (such as RT–qPCR and western blotting) in capturing small differences in transcript or protein expression.

Expression of glucose transporter genes and fatty acid oxidation gene signature in single-cell RNA sequencing

To test the expression of *Slc2a4* and other glucose transporter genes, we retrieved the raw counts from our most recent single-cell RNA sequencing dataset from the SVZ neurogenic niche from young and old mice[70] and used a subset of the data containing only the control (sedentary) animals across young and old ages (i.e. O_Control and Y_Control in the AgeCond metadata column). We normalized the counts data by dividing each cell by its total expression, scaling up to 10^5 total counts per cell, and then taking the log-transform of the normalized counts with an added pseudocount. For comparisons across cell types, we used the pre-existing cell-type annotations: Astrocyte_qNSC, aNSC_NPC and Neuroblast[70]. For comparisons across age, we compared old (O_Control) and young (Y_Control) animals using the pre-existing age annotations in the dataset[70]. For statistical comparisons of the mean expression across conditions, we used the two-sample Welch's *t*-test from stat_compare_means(). Welch's *t*-test is designed for unequal population variances. To compute the log fold change, we divided the average expression in the old cells by the average expression in young cells and then took the $\log_2$-transform of the resulting ratio. To compute the fatty acid oxidation gene signature, we summed the expression of the 19 genes from the fatty acid oxidation signature published in ref. 95 for each cell in the published single-cell RNA sequencing dataset from SVZ neurogenic niches of young and old mice[70]. We then compared the fatty acid oxidation gene signature levels across old and young qNSCs/astrocytes using the two-sample Welch's *t*-test, which is designed for unequal population variances.

Expression of *Slc2a4* RNA in bulk RNA sequencing (in vitro)

To test the expression of *Slc2a4* in vitro, we retrieved the RNA sequencing normalized counts from in vitro qNSCs and aNSCs from a published dataset[51]. To calculate significance between qNSCs and aNSCs, we used a two-sided Mann–Whitney test.

Glucose uptake assays

For qNSCs, we seeded 40,000 cells per well and for aNSCs we seeded 10,000 cells per well (aNSCs do not stick to the plate as well and will double every 16–24 h, so we seeded fewer cells to achieve similar density to qNSCs at the time of analysis) on PDL (Sigma-Aldrich, P6407) pre-coated 96-well plates, performing the assay 3 days after seeding. Duplicate wells were seeded and used for cell count normalization at time of glucose uptake assay. For knockout experiments, 1×10^5 qNSCs were plated per well on PDL pre-coated 96-well plates in qNSC medium 6 days before infection with lentivirus to express sgRNA, for which 1 µl of concentrated virus was added to the culture medium for 16 h to achieve about 100% infection of the cells. We then assessed glucose uptake either 4 days or 8 days after infection using two different types of assays (see below).

Colorimetric glucose uptake assay. For the colorimetric glucose uptake assay (Glucose Uptake-Glo Assay, Promega, J1342; Fig. 4f,h), experiments were performed according to the manufacturer's protocol, with the following details. Cells were pre-treated for 1 h of qNSC/aNSC culture medium without glucose. Culture medium was then

replaced with 50 µl of qNSC/aNSC medium containing 1 mM 2-DG (provided in the Glucose Uptake-Glo kit from Promega (J1342)) reagent for 10 min in an incubator (humidified, 37 °C, 5% CO_2). The 2-DG medium was then removed and 50 µl of PBS was added before carrying out the remainder of the assay according to the manufacturer's protocol. All media treatments and reagent exchanges were pre-aliquoted into an empty 96-well plate, such that we could add the treatment to entire rows of cells at once using a multi-channel pipette to ensure that the duration of treatment was equivalent across different cell types and ages. The luminescence of the cells was measured with 0.5 s readings using a Varioskan LUX multimode plate reader. Owing to different treatments having effects on cell numbers, plate readings in some cases (mentioned in figure legends) required normalization to the cell counts (Countess II cell counter, Thermo Fisher Scientific) based on duplicate wells. We performed glucose uptake experiments on different numbers of NSCs and observed a linear correlation between relative light units and cells plated.

Fluorescent glucose uptake assay. For the fluorescent 2-NBDG glucose uptake assay (fluorescent 2-NBDG [2-(*N*-(7-nitrobenz-2-oxa-1,3-diazol-4-yl)Amino)-2-deoxyglucose] (Fisher, N13195; Extended Data Fig. 6f), cells were placed in glucose-free medium for 1 h and then treated with 200 µM 2-NBDG for 30 min at 37 °C, and then analysed by flow cytometry at excitation/emission maxima of around 465/540 nm, with DAPI added in the medium to eliminate dead cells.

Assessing GLUT4 depletion efficiency at the protein level in vitro

Western blot to assess GLUT4 depletion efficiency at the protein level. Young aNSCs were seeded onto PDL-coated 10 cm plates at a density of 1×10^7 cells per plate and transferred into qNSC medium. Medium was changed every 2 days. After 4 or 5 days in qNSC medium, qNSC cultures were infected with lentivirus expressing control sgRNAs or *Slc2a4* sgRNAs (5 sgRNAs). Seven days after infection, 1.0 µg ml^{-1} puromycin (Sigma-Aldrich, P8833) was added to the cultures for 3 days, with medium changes every day, to select for infected cells. Then, the cells were washed with PBS and incubated on ice with ice-cold 1× lysis buffer (50 mM Tris-HCl, pH 8, 150 mM NaCl, 0.5% sodium deoxycholate and 0.5% Triton-X 100) and 1× protease inhibitor (Thermo Fisher Scientific, 87786) for 10 min and cells were scraped off of the plate. Lysates were centrifuged at 10,000*g* for 10 min at 4 °C. The supernatant was removed and preserved, then the protein concentration was quantified using a BCA assay (Thermo Fisher Scientific 23225). To load the samples, 4× LDS buffer (Invitrogen NP007) with 1 mM DTT (Sigma-Aldrich 10197777001) was added to lysates with equal concentrations of protein and the mix was incubated at 95 °C for 7 min; 25 µg of protein was added to each lane. Proteins were separated by SDS–PAGE in MOPS buffer (Invitrogen NP0001) on precast 4–12% Bis-Tris polyacrylamide gels (InvitrogenNP0323BOX). Proteins were transferred onto nitrocellulose membranes. Membranes were incubated for 30 min at room temperature in blocking buffer (PBS + 3% w/v non-fat dry milk + 0.2% Tween-20). Given that GLUT4 and the loading control (β-actin) have a similar molecular weight, we performed western blotting in a sequential manner (first GLUT4 and then β-actin). Primary antibodies to GLUT4 (1:500, Invitrogen PA1-1065) were diluted in blocking buffer and incubated overnight at 4 °C. After three washes in PBS + 0.2% Tween-20, goat anti-rabbit 800CW (1:10,000, Li-Cor 925-32211) in blocking buffer were incubated for 1 h at room temperature and washed 3 times in PBS + 0.2% Tween-20. Detection was performed on a Li-Cor Odyssey FC imaging system with the 800 channel for 10 min. Then primary antibodies to β-actin (1:40,000, Abcam ab6276) as a loading control were added for 1 h at room temperature and washed 3 times in PBS + 0.2% Tween-20. Goat anti-mouse 680CW (1:10,000, Li-Cor 925-68070) in blocking buffer was incubated for 1 h at room temperature and washed 3 times in PBS + 0.2% Tween-20. Detection was performed on a Li-Cor Odyssey FC imaging system with the 700 channel for 30 s. We used ImageJ to quantify the intensity of the GLUT4 and β-actin bands, and the intensity of the GLUT4 band was divided by the intensity of the corresponding β-actin band for each sample. We note that we used different GLUT4 antibodies used for immunofluorescence and western blot experiments because the GLUT4 antibodies used for immunofluorescence did not work for western blotting. This is most likely due to the fact that proteins are in their native form in immunofluorescence experiments but are denatured in western blot experiments. Both GLUT4 antibodies for immunofluorescence and western blotting were both validated using *Scl2a4* (GLUT4 knockout) (Fig. 3a–d and Extended Data Fig. 6j).

FACS to assess GLUT4 depletion efficiency at the protein level. We plated NSCs on PDL-coated 24-well plates at the density of 3×10^5 cells per well and added qNSC medium for 4 days. After 4 days in quiescence, lentivirus expressing control sgRNAs or sgRNAs to *Slc2a4* (5 sgRNAs) was added to qNSCs for overnight infection, and the cells were kept in qNSC medium for another 6 days. After 6 days (to leave time for infection and knockout to occur), the cells were dissociated with Accutase and placed in 500 µl of medium in a 24-well format. FACS was performed by mixing the primary GLUT4 antibody (R&D Systems, MAB1262) at a 5:1 ratio with secondary anti-IgG AlexaFluor647 for 10 min on ice, in the dark. The antibody mix was added to live cells in culture at a dilution factor of 200× (502.5 µl total volume) and incubated in a cell culture incubator (37 °C, 5% CO_2) for 30 min. The cells were then fixed by adding 500 µl of PBS + 1% PFA to each well, without shaking the cells. Cells were incubated at room temperature for 20 min in the dark, and then analysed by FACS (BD, LSRFortessa). FACS quantification was done by gating first on mCherry$^+$ cells (infected cells).

ECAR and OCR

To measure ECAR and OCR, we seeded 80,000 NSCs into qNSC medium in a PDL pre-treated well of a 96-well plate. The cells were maintained in quiescence for 4 days with medium exchanges at 24 and 72 h after seeding. The cells were then treated with unconcentrated equal titre lentivirus (with control sgRNAs or sgRNAs to *Scl2a4*) for 16 h of overnight infection. The cells were placed back into qNSC medium for 48 h before running the metabolic assay. For ECAR, assays were run according to manufacturer's protocol (Glycolysis assay, Abcam, Ab197244), with the following parameters. The cells were placed in a CO_2-free incubator at 37 °C for 3 h before running the assay. Fluorescence was measured using a Tecan Spark plate reader with the following settings: instrument was pre-warmed to 37 °C 1 h before the run, the run mode parameters were as follows: kinetic, kinetic duration 90 min, interval time 1 min and 30 s, excitation wavelength 380, excitation bandwidth 20, emission wavelength 615, emission bandwidth 10. The slope of the fluorescence detected over the period of linear increase was calculated for each sample. For OCR, assays were run according to the manufacturer's protocol (Extracellular Oxygen Consumption Assay, Abcam, Ab197243) with the following parameters. The extracellular O_2 consumption reagent was used at 1/15 dilution (10 µl added to 150 µl of sample in a 96-well plate). High-sensitivity mineral oil was pre-warmed to 37 °C 30 min before use, and 2 drops were used for each well before running the assay on plate reader. Fluorescence was measured using a Tecan spark plate reader with following measurements: excitation 380 ± 20 nm, emission 650 ± 20 nm, kinetic duration 1 h and 30 min, interval time 1 min and 30 s. The slope of the fluorescence detected over the period of linear increase was calculated for each sample.

Transient glucose starvation

NSCs were placed in qNSC medium for 4 days, exposed to lentivirus to express sgRNAs targeting *Slc2a4* or unannotated genomic regions (control). Then 6 days after infection, the cell medium was replaced with standard complete qNSC medium with glucose or modified to have no glucose (Neurobasal A medium, Thermo Scientific, A2477501, no D-glucose, no sodium pyruvate, supplemented

with 1× sodium pyruvate, Fisher Scientific, 11-360-070) for 48 h, at which point the medium was replaced with standard complete aNSC medium (with normal glucose concentration (4,500 mg l^{-1}) in Neurobasal A medium, Thermo Fisher 10888-022) and the cells were allowed to activate for 4 days before intracellular FACS analysis with Ki67.

Effect of 2-DG on young and old NSC activation

To test the effect of 2-DG on young and old NSC activation, we performed qNSC activation experiments in a 24-well plate format. Primary cultures of NSCs were derived from a pool of 2 young (3–4 months old) or old (18–21 months old) mice (1:1 mix of male and female). We seeded 2×10^5 NSCs in each well of a 24-well plate. After 4 days in qNSC medium (with qNSC medium changes every 2 days), 2-DG (2 mM final concentration, Sigma, D8375) was added to the medium for 36 h of treatment, with one exchange at the 24-h time point. After 36 h of treatment, the cells were washed 1× in PBS and then transitioned to aNSC medium for activation. aNSC medium was exchanged once after 48 h and then Ki67 intracellular FACS was performed at day 4 after treatment to assess NSC activation efficiency as described above. *P* values were determined by two-tailed Mann–Whitney test.

Statistical analyses

We did not perform randomization, but for all experiments, young and old conditions were processed in an alternate manner rather than in two large groups to minimize the group effect. We did not perform power analyses, although we did take into account previous experiments to determine the number of animals needed. To calculate significance for experiments, all tests were two-sided Mann–Whitney tests, unless otherwise indicated. Results from individual experiments and all statistical analyses are included in the source data.

Reporting summary

Further information on research design is available in the Nature Portfolio Reporting Summary linked to this article.

Data availability

The sequencing data generated in this study have been deposited into the NCBI's Gene Expression Omnibus with accession GSE189251. Figs. 1, 2 and 4 and Extended Data Figs. 1, 2 and 4 of this study are based on the raw data, which can be found under this accession number. Raw sequences for screen libraries are provided as FASTQ files and csv count files. For GO searches with EnrichR, we searched the following databases: GO Biological Process 2018 (https://maayanlab.cloud/Enrichr/geneSetLibrary?mode=text&libraryName=GO_Biological_Process_2018); Molecular function 2018 (https://maayanlab.cloud/Enrichr/geneSetLibrary?mode=text&libraryName=GO_Molecular_Function_2018); and Cellular components 2018 (https://maayanlab.cloud/Enrichr/geneSetLibrary?mode=text&libraryName=GO_Cellular_Component_2018). The Online GEne Essentiality database can be found at Online GEne Essentiality (https://v3.ogee.info/#/home)[92] and the Core Essential Genes 2 can be found in Supplemental Table 2 from ref. 91 (https://doi.org/10.1534/g3.117.041277). The single-cell dataset used for analysis can be accessed at Zenodo (https://doi.org/10.5281/zenodo.7338746)[96]. Source data are provided with this paper.

Code availability

The code used to analyse screen data in the current study is available from the GitHub repository for this article (https://github.com/Ruetz/Cas9_aging_NSC).

85. Hales, C. M. et al. Changes in the detergent-insoluble brain proteome linked to amyloid and tau in Alzheimer's disease progression. *Proteomics* **16**, 3042–3053 (2016).
86. Holstege, H. et al. Characterization of pathogenic *SORL1* genetic variants for association with Alzheimer's disease: a clinical interpretation strategy. *Eur. J. Hum. Genet.* **25**, 973–981 (2017).
87. Yashin, A. I. et al. Genetics of aging, health, and survival: dynamic regulation of human longevity related traits. *Front. Genet.* **6**, 122 (2015).
88. Dulken, B. W. et al. Single-cell analysis reveals T cell infiltration in old neurogenic niches. *Nature* **571**, 205–210 (2019).
89. Chen, E. Y. et al. Enrichr: interactive and collaborative HTML5 gene list enrichment analysis tool. *BMC Bioinformatics* **14**, 128 (2013).
90. Kuleshov, M. V. et al. Enrichr: a comprehensive gene set enrichment analysis web server 2016 update. *Nucleic Acids Res.* **44**, W90–W97 (2016).
91. Hart, T. et al. Evaluation and design of genome-wide CRISPR/SpCas9 knockout screens. *G3 (Bethesda)* **7**, 2719–2727 (2017).
92. Gurumayum, S. et al. OGEE v3: Online GEne Essentiality database with increased coverage of organisms and human cell lines. *Nucleic Acids Res.* **49**, D998–D1003 (2021).
93. Bloh, K. et al. Deconvolution of complex DNA repair (DECODR): establishing a novel deconvolution algorithm for comprehensive analysis of CRISPR-edited Sanger sequencing data. *CRISPR J.* **4**, 120–131 (2021).
94. Bankhead, P. et al. QuPath: open source software for digital pathology image analysis. *Sci. Rep.* **7**, 16878 (2017).
95. Aiderus, A., Black, M. A. & Dunbier, A. K. Fatty acid oxidation is associated with proliferation and prognosis in breast and other cancers. *BMC Cancer* **18**, 805 (2018).
96. Sun, E. D. Processed single-cell RNA-seq data for exercise rejuvenation intervention on mouse subventricular zone [data set]. *Zenodo* https://doi.org/10.5281/zenodo.7338746 (2022).

Acknowledgements We thank L. Xu, J. Miklas, F. Boos, R. Nagvekar, D. Heinzer and all members of the Brunet Laboratory for their input on the project and providing feedback on the manuscript; G. A. Reeves for independent code checking of the manuscript; J. Butterfield, J. Ramirez-Matias and M. Hauptschein for help with mouse husbandry and genotyping; J. Long and K. Svensson with their advice regarding glucose metabolism; and X. Ji for help with sequencing the in vivo screen libraries. This work was supported by P01AG036695 (A.B.), R01AG056290 (A.B.), Stanford Brain Rejuvenation Project (A.B.) and a Larry L. Hillblom Foundation Postdoctoral Fellowship (T.J.R.).

Author contributions T.J.R. designed the project with help from A.B., performed all experiments and computationally analysed all results unless otherwise indicated. A.N.P. investigated screen outliers and essential genes and tested knockout efficiency at the genomic level and by western blotting. C.M.K. helped with NSC in vitro and in vivo immunofluorescence experiments, including virus production, mouse EdU injections, mouse perfusions, brain cryosectioning and processing for immunofluorescence and imaging. S.D.G. helped with individual validation in vitro. B.M. assisted with the in vitro genome-wide screen experiments and assisted stereotaxic brain surgeries for in vivo screen experiments. E.D.S. helped with single-cell RNA sequencing re-analysis. J.N. helped with glucose uptake experiments. R.W.Y. helped establish the lentiviral approaches for gene knockouts in NSCs, and trained C.M.K. on mouse perfusions and cryosectioning. D.S.L. helped establish the qNSC culture activation model from young and old mice. D.W.M. provided feedback on the CasTLE analysis and helped design the in vivo screening experiments, including the sgRNA controls. C.K.T. provided the plasmids and protocols for cloning sgRNAs. A.L. provided the plasmid libraries and technical input for genome-wide sgRNA lentivirus production. M.C.B. provided the sgRNA plasmid libraries, gave input on screen design, technical troubleshooting and interpretation of screen results. T.J.R. and A.B. wrote the manuscript with help from A.N.P., and all authors provide comments.

Competing interests T.J.R. is a co-founder of ReneuBio. M.C.B. has outside interest in DEM Biopharma and Stylus Medicine. A.B. is a member of the scientific advisory board of Calico.

Additional information

Supplementary information The online version contains supplementary material available at https://doi.org/10.1038/s41586-024-07972-2.

Correspondence and requests for materials should be addressed to Anne Brunet.

Peer review information *Nature* thanks the anonymous reviewers for their contribution to the peer review of this work. Peer reviewer reports are available.

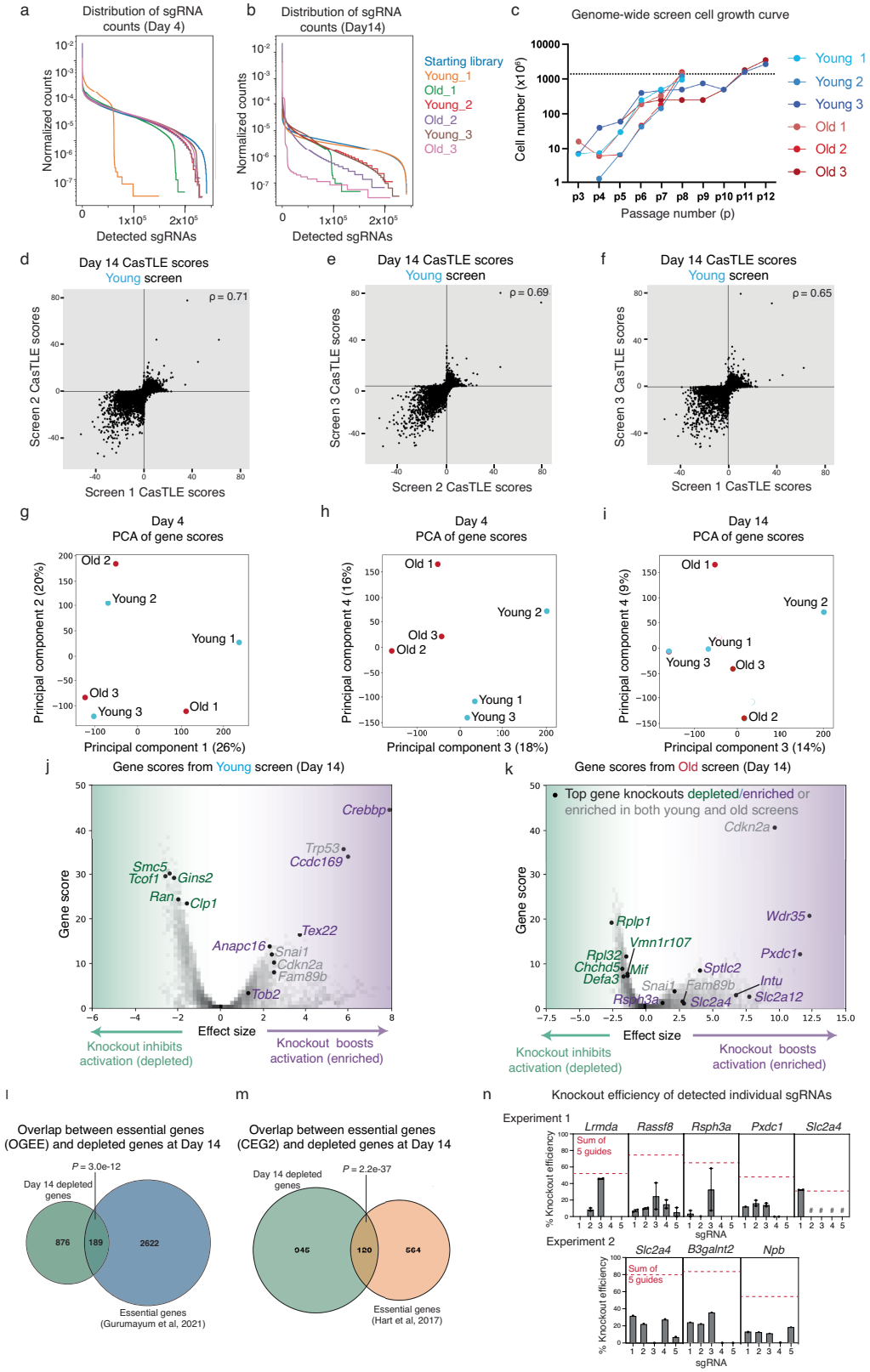

Extended Data Fig. 1 | See next page for caption.

Extended Data Fig. 1 | Genome-wide screen quality control. a, **b**, Normalized count matrices of all sgRNA counts across samples at Day 4 (**a**) or Day 14 (**b**). **c**, Growth curves with number of cells at each passage (p3-p12) for primary cultures of NSCs from young (3-4 months) and old (18–21 months) mice used for the genome-wide screens. Dots represent cell counts for the sample at each passage ($x10^6$). Dotted line at 1.4×10^9 represents the required number of cells for each biological replicate. **d**-**f**, Pairwise comparison of CasTLE scores across young screen samples at Day 14. Correlation plots between Screen 1 and Screen 2, Screen 2 and Screen 3; Screen 1 and Screen 3. Spearman ρ is indicated. **g**-**i**, Principal Component Analysis (PCA) performed on all gene scores of the three independent screens at Day 4 (g,h) and Day 14 (i): Young 1, 2, 3 (blue) and Old 1, 2, 3 (red), with Principal Components 1 vs. 2 (**g**) and Principal Components 3 vs. 4 (**h**,**i**). **j**,**k**, Volcano plots of example screen results (screen 1) at Day 14 for young (**j**) or old NSCs (**k**), showing gene scores as a function of effect size. Each dot represents one gene. Labelled dots are top ranking gene knockouts in at least 2 of the 3 independent screens (FDR < 0.1). Selecting genes that intersect screen 1 (day 4 or 14) with screen 2 (day 4 or 14) that boost NSC activation (purple, corresponding to enriched sgRNAs) or impede NSC activation (green, corresponding to depleted sgRNAs) in an age-dependent manner or gene knockouts that boost activation regardless of age (grey, corresponding to enriched sgRNAs). See Supplementary Table 1 for complete list of gene scores. **l**, Comparison of significantly depleted genes (FDR < 0.1) in genome-wide screen (Day 14) and essential genes identified from Online GEne Essentiality database (OGEE)[92]. **m**, Comparison of significantly depleted genes (FDR < 0.1) in genome-wide screen (Day 14) and essential genes identified from Core Essential Genes 2 (CEG2)[91]. **n**, Validation of gene knockout efficiency at the genomic level. qNSCs were infected with lentivirus expressing sgRNAs targeting individual genes (5 sgRNAs per gene) and genomic DNA was extracted. Percentage of knockout was quantified by sequencing PCR products followed by DECODRv3.0. Top: Experiment 1. Dot plot of the percentage of knockout for n = 2 independent primary NSC cultures, each derived from 2 mice (one young, one old). Connecting line indicates range. Bottom: Experiment 2. Dot plot of the percentage of knockout for n = 1 independent primary NSC culture derived from 1 mouse (young). Each dot represents the percentage knockout for one sgRNA. #: knockout detected by DECODRv3.0, but with low confidence ($r^2 < 0.6$) (see Source Data). No data point: knockout not detected by DECODRv3.0 (see Source Data). Dotted red line: sum of knockout percentages for high confidence and detected knockouts. See Extended Data Fig. 6h–m for genomic knockout examples and knockout efficiency by western blot and FACS for *Slc2a4* (GLUT4).

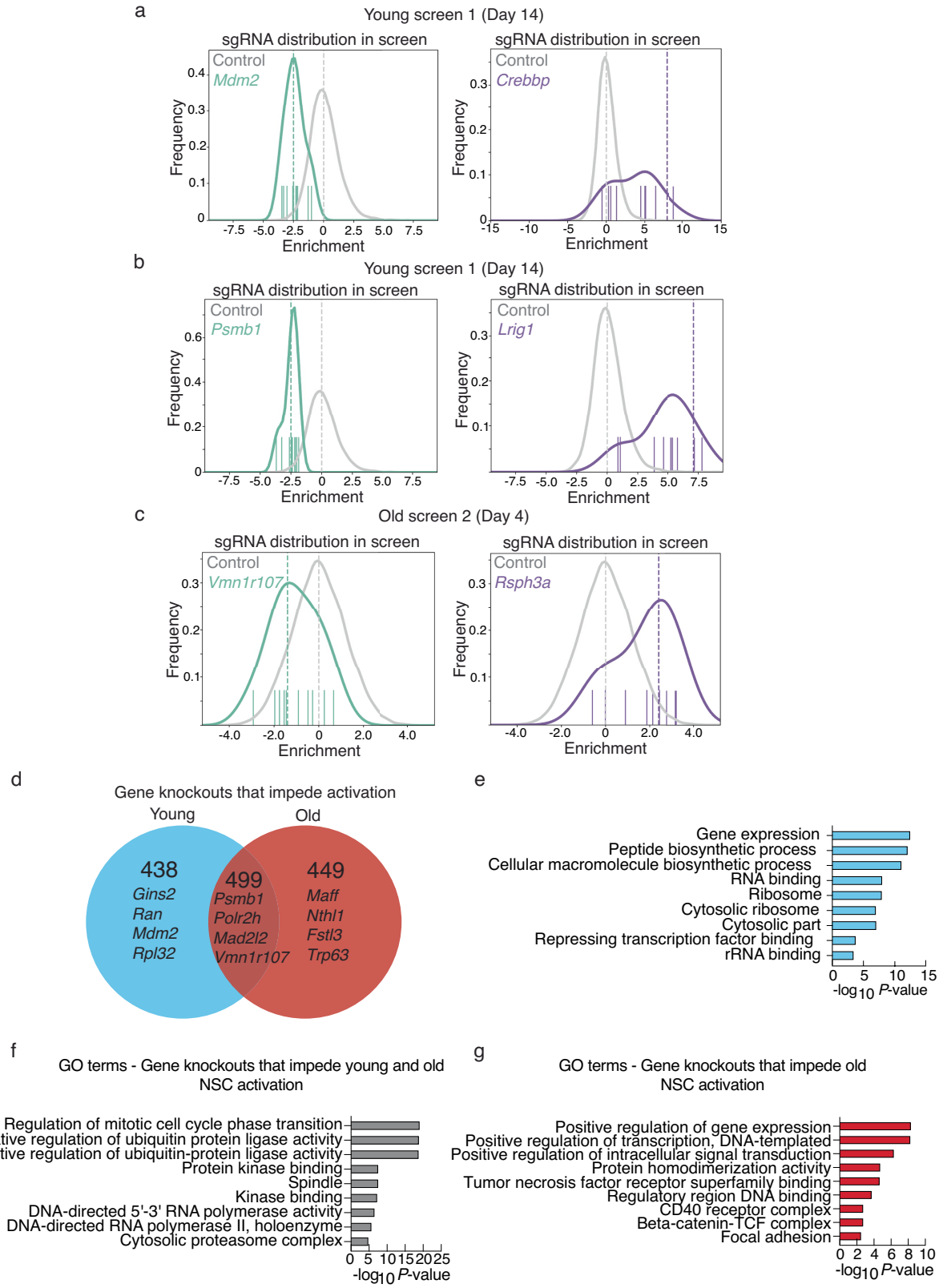

Extended Data Fig. 2 | See next page for caption.

Extended Data Fig. 2 | Example top sgRNAs counts from gene knockouts enriched or depleted in genome-wide screens and Gene Ontology analysis of gene knockouts that impede activation. a-**c**, Histograms plotting the relative enrichment and frequency of each sgRNA targeting a gene of interest or the control sgRNA pool (control), comparing the starting sgRNA plasmid library to the screen result. Enriched sgRNAs (purple) and depleted sgRNAs (green). Hashed line indicates the CasTLE computed enrichment effect size for sgRNA targeting the gene of interest and control sgRNA pool. Colored dashes above the x-axis represent each of the sgRNAs targeting the gene of interest and their relative enrichment. **d**, Venn diagram of all gene knockouts that impede NSC activation in at least 2 of the 3 independent screens (FDR < 0.1). Selecting genes that intersect screen 1 (Day 4 or 14) with screen 2 (Day 4 or 14) in young (blue) or old NSCs (red). **e**-**g**, Gene Ontology (GO) terms associated with gene knockouts that impede young (**e**) NSC activation, impede activation regardless of age (**f**), or impede activation of old (**g**) NSCs. For complete list of GO terms, see Supplementary Table 2. Gene sets selected based on FDR < 0.1 in at least 2 of the 3 independent screens. GO terms assessed using EnrichR focusing on the "cell component", "molecular function" and "biological process" libraries. *P*-value calculated by EnrichR using a one-sided Fisher's exact test.

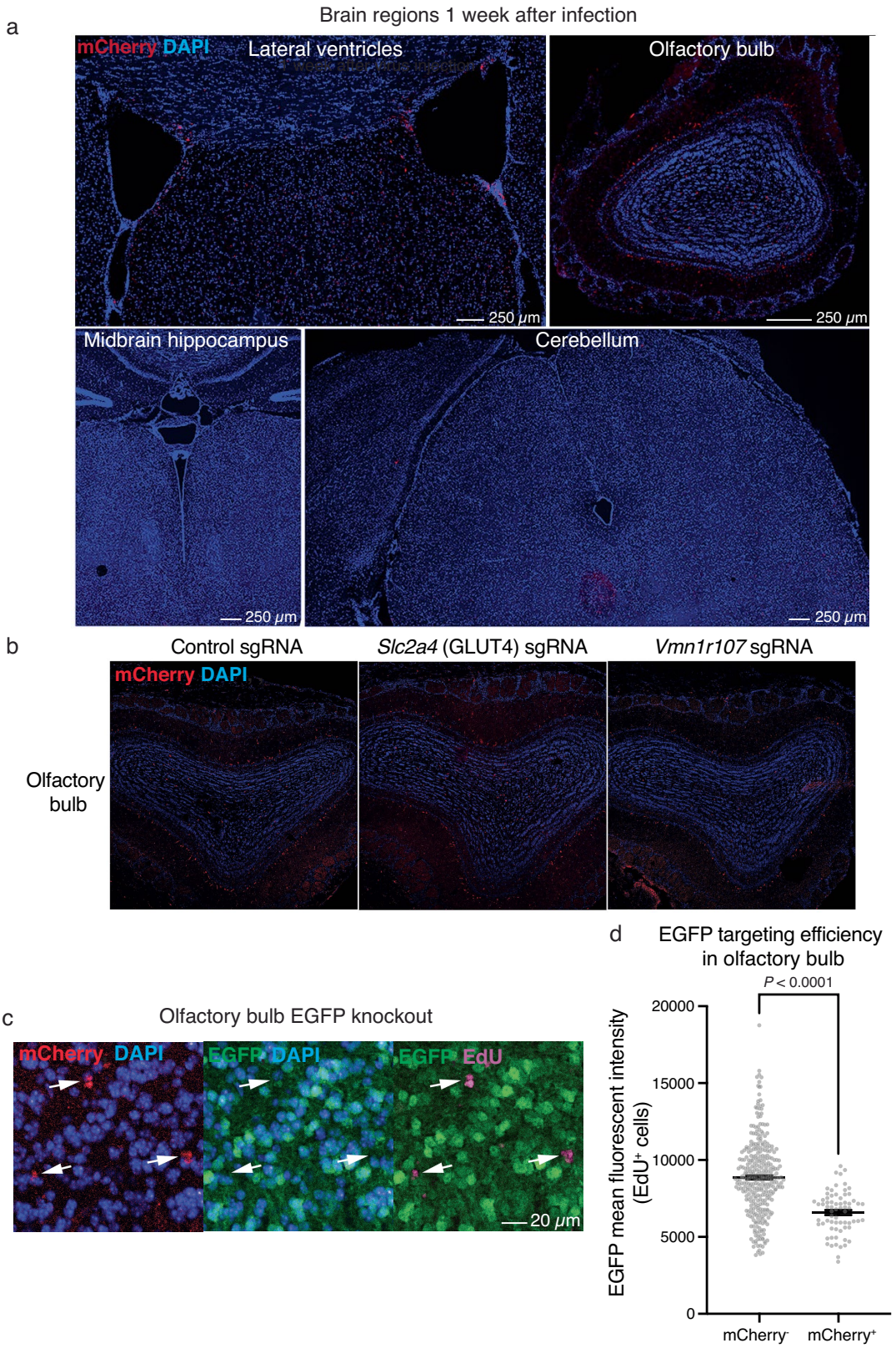

Extended Data Fig. 3 | See next page for caption.

Extended Data Fig. 3 | Efficiency of in vivo lentiviral injection and knockout. **a**, Immunofluorescence images of sections of the lateral ventricles and subventricular zones (SVZs), olfactory bulb (OB), midbrain hippocampus and hindbrain cerebellum regions of old (22 months old) female Cas9 mice, 1 week after injection of lentivirus expressing mCherry reporter and sgRNAs. One experiment; representative of 3 independent experiments. mCherry reporter (lentivirus-infected cells, red) and cell nuclei (DAPI, blue). **b**, Immunofluorescence images of sections of mCherry expression in the olfactory bulb of old (21 months old) female Cas9 mice, 5 weeks after injection of lentivirus expressing mCherry reporter and sgRNAs. One experiment; representative of 3 independent experiments. mCherry reporter (lentivirus-infected cells, red) and cell nuclei (DAPI, blue). **c**, Zoomed-in immunofluorescence images of sections of olfactory bulb from old (22 months old) female Cas9 mice, 5 weeks after injection of lentivirus expressing sgRNA targeting the EGFP reporter present in Cas9 mice directly into the lateral ventricles. Mice were injected with EdU once per week, starting one week after virus injection, for 4 weeks. mCherry reporter (lentivirus-infected cells, red), EGFP reporter (present in Cas9 mice, green), EdU (newborn cells, magenta) and cell nuclei (DAPI, blue). One experiment; quantification in d. **d**, Quantification of EGFP mean fluorescent intensity in non-infected ($mCherry^-$) and infected ($mCherry^+$) newborn cells (EdU^+) in the olfactory bulb, 5 weeks after injection of lentivirus to express sgRNA targeting EGFP into the lateral ventricle. Mean +/−SEM of EGFP fluorescence intensity in EdU+ cells for n = 354 $mCherry^-$ cells and n = 69 $mCherry^+$ cells from 1 old (22 month) female mouse. Each dot represents one cell. *P*-value: two-tailed Mann-Whitney test.

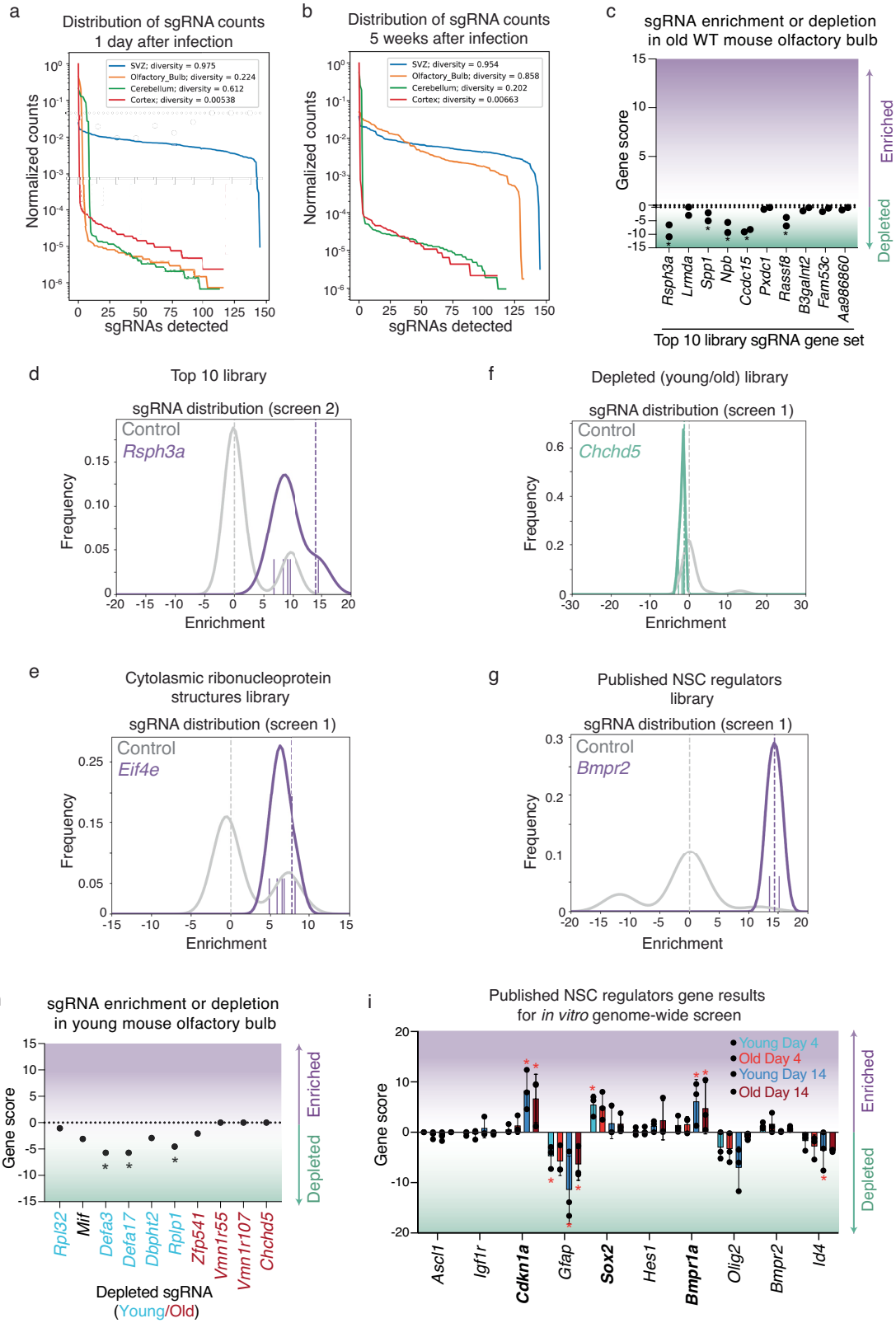

Extended Data Fig. 4 | See next page for caption.

Extended Data Fig. 4 | In vivo screen quality control, wild-type controls, example genes, young mouse screen. a, **b**, Normalized count matrices of all sgRNA counts across samples at 24 h (**a**) or 5 weeks (**b**) post virus injection. **c**, Olfactory bulb sgRNA enrichment CasTLE analysis results showing gene scores of the Top 10 gene pool, 5 weeks after injection of lentivirus expressing sgRNAs targeted to these genes directly into the lateral ventricles of wild-type (WT) old (20-21 months old) male mice. Gene scores were computed by comparing the olfactory bulb sgRNA counts 5-week post injection and the SVZ sgRNA counts from an independent mouse sequenced 24 h after injection. Each dot represents gene score from an independent mouse. *: gene hits with a 95% confidence interval that did not contain 0 as computed by CasTLE analysis, in at least one of the 2 independent mice. **d**-**g**, Histograms plotting the relative enrichment and frequency of each sgRNA targeting a gene of interest or the control sgRNA pool, comparing the starting sgRNA library in the SVZ at 24 h post infection to the olfactory bulb sgRNA counts at 5 weeks post injection. Example top ranked genes. Hashed line indicates the CasTLE computed enrichment effect size for targeted gene and control pool. Colored dashes above the x-axis represent each of the sgRNAs targeting the gene of interest and their relative enrichment. **h**, CasTLE gene scores for 10 gene knockouts (depleted in young/old in vitro screens) in young (3 months old) female Cas9 mice olfactory bulbs. The library of 10 genes was injected into 1 young Cas9 mouse, which was left for 5 weeks and then the olfactory bulb sgRNAs were sequenced. Olfactory bulb sgRNA enrichment was computed with CasTLE by comparison to the 24-hour SVZ sequenced sample. Dot plot showing mean of CasTLE score in 1 mouse. Each dot represents gene score from one mouse. *: gene hits with a 95% confidence interval that did not contain 0 as computed by CasTLE analysis. **i**, Comparison between "Published NSC regulators" hits in in vitro and in vivo screens. Mean +/-SD of gene scores for our 3 in vitro screens were plotted for 10 genes among "Published NSC regulators" hits. Each dot represents gene score for one screen. *P*-values: two-tailed Mann-Whitney test. Bold: gene knockouts that were similar in vitro and in vivo screens. See also Supplementary Table 3.

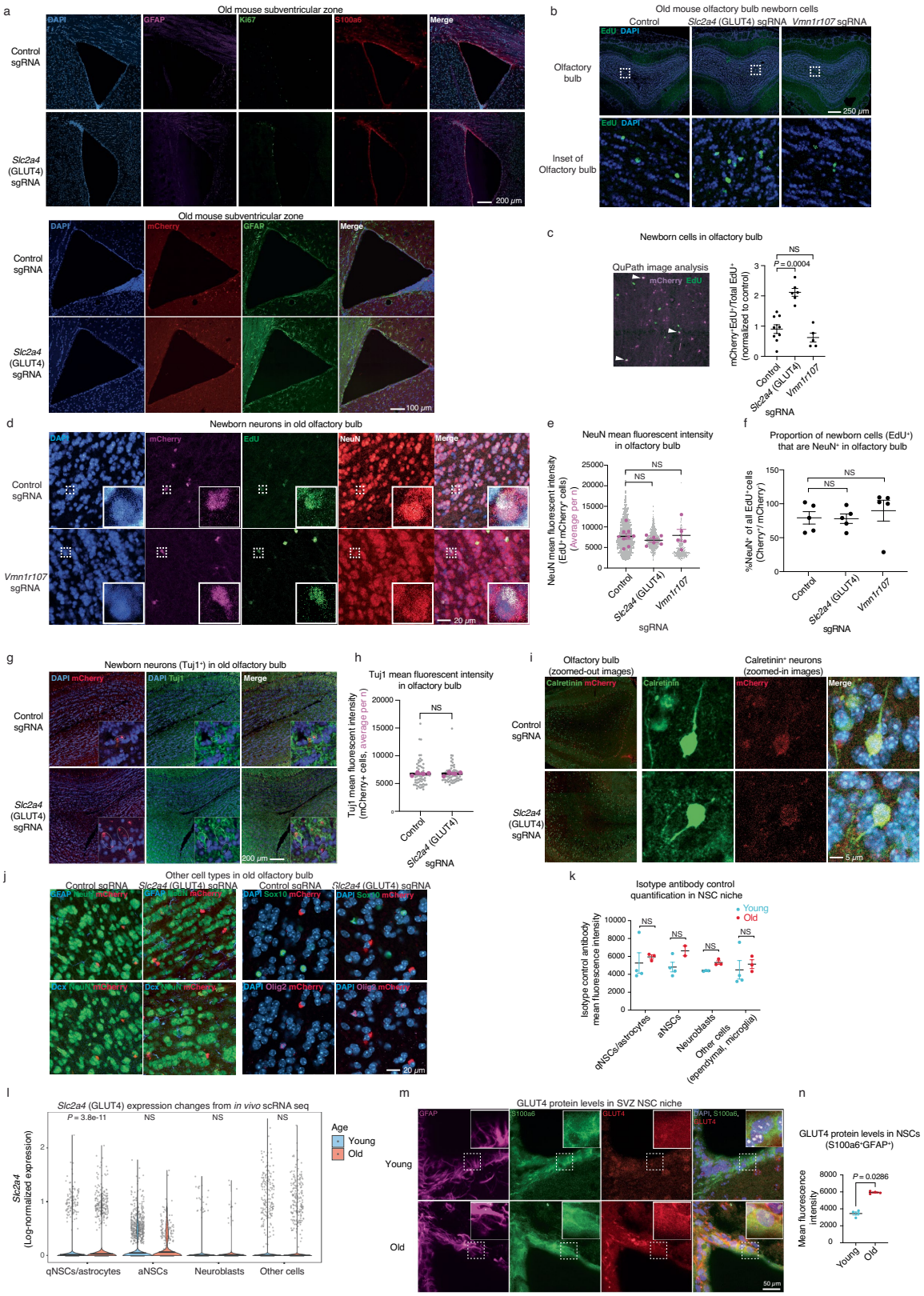

Extended Data Fig. 5 | See next page for caption.

Extended Data Fig. 5 | GLUT4 knockout efficiency in vivo, proportion of newborn cells that become neurons, other cell types in the olfactory bulb, and GLUT4 expression with aging. a, Top panel: immunofluorescence images of SVZ sections from old (22 months old) female Cas9 mice, 5 weeks after injection with lentivirus expressing *Slc2a4* (GLUT4) sgRNAs directly into the lateral ventricles. One experiment; representative of 3 independent experiments. DAPI (nuclei, blue), GFAP (qNSCs/astrocytes, magenta), Ki67 (proliferative cells, green), S100a6 (NSCs, red), merge image. Bottom panel: immunofluorescent images of sections of the SVZ from the same mice as in top panel. DAPI (nuclei, blue), mCherry (lentivirus-infected cells, red), and GFAP (qNSCs/astrocytes, green). **b**, Immunofluorescence images of olfactory bulb (OB) sections from old (~20 months old) male Cas9 mice, 5 weeks after injection of lentivirus expressing control (unannotated genomic regions), *Slc2a4* (GLUT4) or *Vmn1r107* sgRNAs directly into the lateral ventricles. One experiment; representative of 3 independent experiments. Mice were injected with EdU once per week, starting one week after virus injection, for 4 weeks. EdU (newborn cells, green) and nuclei (DAPI, blue). Zoomed-out images with the dashed white squares representing the insets (top) and zoomed-in images as insets (bottom). **c**, Example image of mCherry (lentivirus-infected cells, magenta) and EdU (newborn cells, green) staining (left panel) and QuPath image quantification of the average number of EdU^+ and $mCherry^+$ cells in the olfactory bulbs, normalized to total EdU^+ cells (right panel) in old Cas9 mice (18–23 months old) (right panel). Mean +/- SEM of the average number of cell counts for one mouse, from 3 serial sections taken at 100 µm intervals across the olfactory bulb pair (normalized to average of control), for n = 9 old mice (4 males, 5 females, 20–23 months) for control sgRNAs, n = 6 old mice (3 males, 3 females, 20 – 23 months) for *Slc2a4* (GLUT4) sgRNAs, and n = 5 old Cas9 mice (3 males, 2 females, 18–22 months) for *Vmn1r107* sgRNAs, over 3 independent experiments. Each dot represents one mouse. *P*-values: two-tailed Mann-Whitney test. **d**, Immunofluorescence images of olfactory bulb sections from old (20 months) male Cas9 mouse, 5 weeks after injection of lentivirus expressing control (unannotated genomic regions) or *Vmn1r107* sgRNAs directly into the lateral ventricles. One experiment; representative of 3 independent experiments. Mice were injected with EdU once per week, starting one week after virus injection, for 4 weeks. EdU (newborn cells, green), mCherry (lentivirus-infected cells, magenta), NeuN (mature neurons, red), and DAPI (nuclei, blue). Dashed white squares: $NeuN^+$ cells that are infected with lentivirus (expressing one of the sgRNAs). Insets: zoomed-in images. **e**, QuPath image quantification of NeuN mean fluorescent intensity in infected ($mCherry^+$) newborn cells (EdU^+) in the olfactory bulb of old Cas9 mice (18–23 months old) (mix of males and females, see Source Data), 5 weeks after injection of lentivirus expressing control (unannotated genomic regions), *Slc2a4* (GLUT4), or *Vmn1r107* sgRNAs directly into the lateral ventricles. Mice were injected with EdU once per week, starting one week after virus injection, for 4 weeks. Mean +/- SEM of the average NeuN fluorescence intensity of all enumerated cells in one mouse, from 3 serial sections taken at 100 µm intervals across the olfactory bulb pair, for n = 9 old Cas9 mice (4 males, 5 females, 20–23 months) for control sgRNAs, n = 6 old Cas9 mice (3 males, 3 females, 20–23 months) for *Slc2a4* (GLUT4) sgRNAs, and n = 5 old Cas9 mice (3 males, 2 females, 18–22 months) for *Vmn1r107* sgRNAs, over 3 independent experiments. Each lavender dot represents one mouse. *P*-values: two tailed Mann-Whitney test. Each grey dot represents a single cell NeuN fluorescence intensity, showing all cells across all samples for each respective treatment. **f**, Image quantification of the percentage of newborn cells (EdU^+) that are also $NeuN^+$, comparing cells with ($mCherry^+$) or without ($mCherry^-$), in control, *Slc2a4*, or *Vmn1r107* sgRNA expression conditions. Mean +/− SEM of the average (%$NeuN^+$) of all cell quantifications from a single mouse for n = 5 old Cas9 mice for each condition, over 3 independent experiments. Each dot represents one mouse. *P*-values: two-tailed Mann-Whitney test. **g**, Immunofluorescence images of olfactory bulb sections from old (20 months old) male Cas9 mouse, 5 weeks after injection of lentivirus expressing *Slc2a4* (GLUT4) sgRNAs directly into the lateral ventricles. Mice were injected with EdU once per week, starting one week after virus injection, for 4 weeks. mCherry (lentivirus-infected cells, red), Tuj1 (neuron marker, green), and DAPI (nuclei, blue). Insets and white ovals: $Tuj1^+$ cells that are infected with lentivirus (expressing one of the sgRNAs targeting *Slc2a4* (GLUT4)). One experiment; representative of 2 independent experiments. **h**, QuPath image quantification of Tuj1 mean fluorescent intensity in infected ($mCherry^+$) newborn cells (EdU^+) in the olfactory bulb of old Cas9 mice (18–21 months old) (mix of males and females), 5 weeks after injection of lentivirus expressing control (unannotated genomic regions), or *Slc2a4* (GLUT4) sgRNAs directly into the lateral ventricles. Mean +/− SEM of the average Tuj1 fluorescence intensity of all enumerated cells in one mouse, sections taken at 100 µm intervals across the olfactory bulb pair for n = 4 old Cas9 mice for each condition, over 2 independent experiments. Each lavender dot represents one mouse. *P*-values: two tailed Mann-Whitney test. Each grey dot represents a single cell Tuj1 fluorescence intensity, showing all cells across all samples for each respective treatment. **i**, Immunofluorescence images of olfactory bulb sections from old (20 months old) male Cas9 mouse, 5 weeks after injection of lentivirus expressing *Slc2a4* (GLUT4) sgRNAs directly into the lateral ventricles. One experiment. Mice were injected with EdU once per week, starting one week after virus injection, for 4 weeks. mCherry (lentivirus-infected cells, red), Calretinin (mature neuron marker, green), and DAPI (nuclei, blue). **j**, Immunofluorescence images of olfactory bulb sections from old (20 months old) male Cas9 mouse, 5 weeks after injection of lentivirus expressing *Slc2a4* (GLUT4) sgRNAs directly into the lateral ventricles. Mice were injected with EdU once per week, starting one week after virus injection, for 4 weeks. Left panels: mCherry (lentivirus-infected cells, red), GFAP (astrocytes, blue, top panels), Dcx (immature neuroblast, blue, bottom panels), NeuN (neurons, green). Right panels: mCherry (lentivirus-infected cells, red), DAPI (nuclei, blue), Sox10 (oligodendrocytes, green, top panels), Olig2 (oligodendrocytes, magenta, lower panels). Note that images are the exact same in the top and lower panels to show the different channels, except for the *Slc2a4* (GLUT4) sgRNA condition for Dcx (lower panel), as there were no Dcx^+ cells (which are very rare) in the same image. One experiment. **k**, QuPath image quantification of the mean fluorescence intensity with an isotype antibody control (mouse IgG) in sections from the SVZ neural stem cell niche from 4 young (3-4 months old) and 3 old (18–21 months old) male Cas9 mice (control for Fig. 3k). Cell types were identified as follows: qNSC/astrocyte ($GFAP^+Ki67^-$), aNSC ($GFAP^+Ki67^+$), Neuroblast ($GFAP^-Ki67^+$) and other cells (ependymal, microglia; $GFAP^-Ki67^-$). Mean +/− SEM of control average fluorescent intensities of each cell type, as identified above, from each mouse, for n = 4 (young qNSCs/astrocytes, young aNSCs, young other cells), n = 3 (young neuroblasts, old qNSCs/astrocytes, old neuroblasts, old other cells), or n = 2 (old aNSCs) Cas9 mice, over 2 experiments. Each dot represents one mouse. *P*-values determined by two tailed Mann-Whitney test. **l**, Violin plots comparing the log-normalized expression of *Slc2a4* (GLUT4) transcripts between young (blue) and old (red) in single cell RNA-seq of qNSCs/astrocytes, aNSCs, neuroblasts, and all other cells from the neurogenic niche[70]. *P*-values determined by two-sided two-sample Welch's t-test. **m**, Representative immunofluorescence images of coronal sections of the SVZ neural stem cell niche from young (3-4 months old) and old (18–21 months old) male Cas9 mice. GLUT4 (red), S100a6 (NSC marker, green), GFAP (NSC and astrocyte marker, magenta), and DAPI (nuclei, blue). Dotted squares: regions with NSCs shown in the insets. Insets: zoomed-in images. **n**, QuPath image quantification of the mean fluorescence intensity of the GLUT4 antibody in $S100a6^+/GFAP^+$ cells quantified from sections of the SVZ neural stem cell niche. Mean +/− SEM of the average fluorescent intensities of cells from one mouse, for n = 4 young (3-4 months old) and n = 4 old (18–21 months old) male Cas9 mice, over 2 independent experiments. Each dot represents a mouse. *P*-values: two tailed Mann-Whitney test.

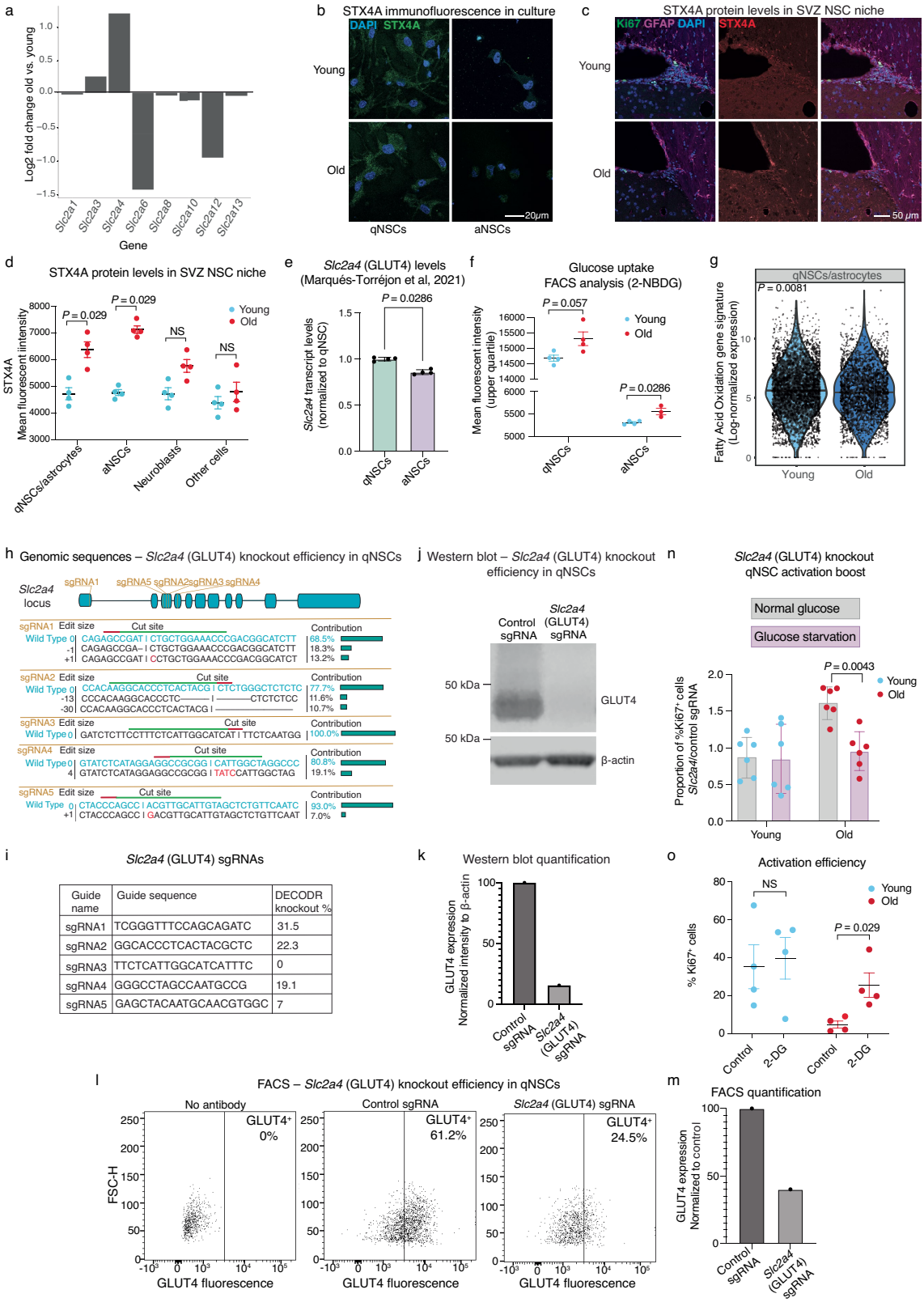

Extended Data Fig. 6 | See next page for caption.

Extended Data Fig. 6 | Glucose transporter expression during aging, STX4A immunofluorescence in vitro and in vivo, *Slc2a4* (GLUT4) knockout efficiency and effects of *Slc2a4* (GLUT4) knockout on qNSC activation in the context of glucose restriction. a, Bar plots showing the log2 fold change in average expression of various *Slc2* transcripts expressed in qNSCs/astrocytes from young and old mice in single cell RNA-seq data[70], where log2 fold changes greater than 0 indicate higher expression in cells of old animals than in young animals. **b**, Immunofluorescence image of STX4A in primary NSC cultures from young (3-4 months old) or old (18–21 months old) mice. NSCs were plated in quiescence NSC media (qNSCs) for 7 days prior to imaging, and NSCs were plated in activated NSC media (aNSCs) 2 days prior to imaging. STX4A (green) and DAPI (nuclei, blue). One experiment; quantification in Fig. 4e. **c**, Representative immunofluorescence images of coronal sections from SVZ NSC niche sections from young (3-4 months old) and old (18–21 months old) Cas9 mice. Ki67 (proliferation maker, green), GFAP (NSC and astrocyte marker, magenta), DAPI (nuclei, blue), and STX4A (red). Cell types were identified as follows: qNSC/astrocytes ($GFAP^+Ki67^-$), aNSCs ($GFAP^+Ki67^+$), Neuroblasts ($GFAP^-Ki67^+$), and other cells (ependymal, microglia; $GFAP^-Ki67^-$). **d**, QuPath image quantification of STX4A mean fluorescence in cells of the neural stem cell niche. Cell types were identified as follows: qNSC/astrocyte ($GFAP^+Ki67^-$), aNSC ($GFAP^+Ki67^+$), Neuroblast ($GFAP^-Ki67^+$) and other cells (ependymal, microglia; $GFAP^-Ki67$). Mean +/− SEM of STX4A mean fluorescence intensity for n = 4 young (~4 months) and n = 4 old (~19 months) Cas9 mice, over 2 independent experiments. Each dot represents one mouse. *P*-values: two tailed Mann-Whitney test. **e**, Expression of *Scl2a4* (GLUT4) transcripts in young (6–8 weeks old) qNSCs and aNSCs in culture from a published RNA-seq dataset[51]. Mean +/− SD from n = 4 qNSC and aNSC cultures. *P*-values: two-tailed Mann-Whitney test. **f**, FACS-based glucose uptake assay with 2NBDG (2-(*N*-(7-Nitrobenz-2-oxa-1,3-diazol-4-yl)Amino)-2-Deoxyglucose) (Sigma, 72987) on primary NSC cultures (qNSCs and aNSCs) from young (3-4-months-old) or old (18–21-months-old) mice. Mean +/− SEM of FACS results from n = 4 (young and old qNSCs, young aNSCs) and n = 3 (old aNSCs) independent NSC cultures, each from a pool of 6 Cas9 mice, 3 males and 3 females. Each dot represents one independent NSC culture. *P*-values: two-tailed Mann-Whitney test. **g**, Violin plots showing the log-normalized expression of all genes in the fatty acid oxidation gene signature[91] across young and old qNSC/astrocyte cells in single cell RNA-seq data[70]. *P*-value: two-sample Welch's t-test. **h**, Top panel: scheme of the *Slc2a4* (GLUT4) locus with the location of sgRNAs 1–5. Bottom panel: genomic sequences for *Slc2a4* (GLUT4) sgRNAs 1–5 from DECODRv3.0 analysis tool indicating the sgRNA target as well as cut site and indel distribution. **i**, Guide sequences used for *Slc2a4* (GLUT4) sgRNAs 1–5 and the DECODRv3.0 knockout percentage for each sgRNA. **j**, GLUT4 knockout efficiency in young (3-4 months) qNSC culture by western blot. Western blot analysis of GLUT4 levels in qNSCs infected with control sgRNA (targeting unannotated regions of the genome) or sgRNA targeting *Slc2a4* (GLUT4), 10 days after infection by lentivirus and 3 days of selection with puromycin. β-actin is used as a loading control. Data from n = 1 (control sgRNAs) and n = 1 (*Slc2a4* (GLUT4) sgRNAs) NSC culture, each derived from one young Cas9 mouse. The western blot was repeated 3 times with similar results. For western blot source data, see Supplementary Fig. 1e. **k**, Quantification of western blot: GLUT4 intensity, normalized to β-actin intensity. **l**, GLUT4 knockout efficiency in primary qNSC cultures by FACS. Intracellular FACS analysis of GLUT4 levels in fixed qNSCs treated with control sgRNA or sgRNA targeting *Slc2a4* (GLUT4), 10 days after lentivirus infection to express sgRNA. No antibody control panel is on the left. Plots show $mCherry^+$ gated cells, GLUT4 fluorescence. **m**, Quantification of FACS data, normalized to control. **n**, Data from Fig. 4i, presented as the boost in qNSC activation ability with *Slc2a4* (GLUT4) knockout, with or without glucose starvation. Mean +/− SEM of NSC activation ability of *Slc2a4* (GLUT4) knockout relative to control, for n = 6 young (3-4 months) or n = 6 old (18–21 months) independent NSC cultures, each derived from a pool of 6 Cas9 mice (3 males, 3 females), over 2 experiments. Each dot represents one independent NSC culture. *P*-values: two-tailed Mann-Whitney test. **o**, Quantification of NSC activation efficiency in cultured NSC from young (3-4 months old) or old (18–21 months old) mice 4 days after transition to aNSC media, as assessed by Ki67 intracellular FACS analysis. NSCs were placed in qNSC media for 4 days. Then the cell media was replaced with qNSC media with or without 2-Deoxy-D-glucose (2-DG) (2 mM) for 48 h, at which point the media was replaced with aNSC media and the cells were allowed to activate for 4 days prior to intracellular FACS analysis with Ki67. Mean +/− SEM of the percentage of $Ki67^+$ cells for n = 4 (young) or n = 4 (old) independent NSC cultures, each derived from a pool of 2 Cas9 mice (1 male, 1 female). Each dot represents one independent NSC culture. *P*-values: two-tailed Mann-Whitney test.

nature portfolio

Corresponding author(s): Anne Brunet

Last updated by author(s): Jul 25, 2024

Reporting Summary

Nature Portfolio wishes to improve the reproducibility of the work that we publish. This form provides structure for consistency and transparency in reporting. For further information on Nature Portfolio policies, see our Editorial Policies and the Editorial Policy Checklist.

Statistics

For all statistical analyses, confirm that the following items are present in the figure legend, table legend, main text, or Methods section.

n/a	Confirmed	
☐	☒	The exact sample size (*n*) for each experimental group/condition, given as a discrete number and unit of measurement
☐	☒	A statement on whether measurements were taken from distinct samples or whether the same sample was measured repeatedly
☐	☒	The statistical test(s) used AND whether they are one- or two-sided *Only common tests should be described solely by name; describe more complex techniques in the Methods section.*
☐	☒	A description of all covariates tested
☐	☒	A description of any assumptions or corrections, such as tests of normality and adjustment for multiple comparisons
☐	☒	A full description of the statistical parameters including central tendency (e.g. means) or other basic estimates (e.g. regression coefficient) AND variation (e.g. standard deviation) or associated estimates of uncertainty (e.g. confidence intervals)
☐	☒	For null hypothesis testing, the test statistic (e.g. *F*, *t*, *r*) with confidence intervals, effect sizes, degrees of freedom and *P* value noted *Give P values as exact values whenever suitable.*
☒	☐	For Bayesian analysis, information on the choice of priors and Markov chain Monte Carlo settings
☒	☐	For hierarchical and complex designs, identification of the appropriate level for tests and full reporting of outcomes
☒	☐	Estimates of effect sizes (e.g. Cohen's *d*, Pearson's *r*), indicating how they were calculated

Our web collection on statistics for biologists contains articles on many of the points above.

Software and code

Policy information about availability of computer code

Data collection	NIS-Elements software (version AR 4.30.02), BD FACSDiva software (version 8.0.1), Zen blue edition (version 3.0)
Data analysis	Data analysis was performed using Python, version 2.7 with Python sklearn.decomposition.PCA module. Code available at https://github.com/Ruetz/Cas9_aging_NSC. Other analysis tools used include Prism (v8, Fiji (v2), EnrichR (https://maayanlab.cloud/Enrichr/), Flowjo (v8), QuPATH (version 0.2.3).

For manuscripts utilizing custom algorithms or software that are central to the research but not yet described in published literature, software must be made available to editors and reviewers. We strongly encourage code deposition in a community repository (e.g. GitHub). See the Nature Portfolio guidelines for submitting code & software for further information.

Data

Policy information about availability of data

All manuscripts must include a data availability statement. This statement should provide the following information, where applicable:

- Accession codes, unique identifiers, or web links for publicly available datasets
- A description of any restrictions on data availability
- For clinical datasets or third party data, please ensure that the statement adheres to our policy

Sequencing data generated in this study have been deposited in NCBI GEO, with accession GSE189251 (https://www.ncbi.nlm.nih.gov/geo/query/acc.cgi?acc=GSE189251).

Figures 1, 2, 4 and Extended Data Figures 1, 2, and 4 of this study are based on the raw data which can be found under this accession number. Raw sequences for screen libraries are provided as FASTQ files and csv count files. For gene ontology searches with EnrichR, we searched the following databases: GO Biological Process 2018 (https://maayanlab.cloud/Enrichr/geneSetLibrary?mode=text&libraryName=GO_Biological_Process_2018), Molecular function 2018 (https://maayanlab.cloud/Enrichr/geneSetLibrary?mode=text&libraryName=GO_Molecular_Function_2018), Cellular components 2018 (https://maayanlab.cloud/Enrichr/geneSetLibrary?mode=text&libraryName=GO_Cellular_Component_2018). The gene essentiality databases can be found here: https://v3.ogee.info/#/home and http://cefg.uestc.cn/ceg. The single-cell dataset used for analysis can be accessed at: https://zenodo.org/doi/10.5281/zenodo.7338745.

Research involving human participants, their data, or biological material

Policy information about studies with human participants or human data. See also policy information about sex, gender (identity/presentation), and sexual orientation and race, ethnicity and racism.

Reporting on sex and gender	N/A
Reporting on race, ethnicity, or other socially relevant groupings	N/A
Population characteristics	N/A
Recruitment	N/A
Ethics oversight	N/A

Note that full information on the approval of the study protocol must also be provided in the manuscript.

Field-specific reporting

Please select the one below that is the best fit for your research. If you are not sure, read the appropriate sections before making your selection.

☒ Life sciences ☐ Behavioural & social sciences ☐ Ecological, evolutionary & environmental sciences

For a reference copy of the document with all sections, see nature.com/documents/nr-reporting-summary-flat.pdf

Life sciences study design

All studies must disclose on these points even when the disclosure is negative.

Sample size	Sample size was decided based on previous experiments and prior literature using similar experimental paradigms as outlined in (Leeman et al. Science Vol 369, Issue 6381). We did not use power analyses and have clearly indicated this in Methods (Statistics section). We have clearly indicated cases where samples from independent experiments were combined, and have included all combined and non-combined data (and associated statistics) in Source Data.
Data exclusions	For the qNSC in vitro activation experiments, on rare occasions the cells did not activate at all (0% Ki67+, in both young and old conditions), and these samples were excluded from further analysis.
Replication	All data in this paper was replicated in at least one other independent experiment (see Source Data), with the exception of Figure 3c-d, Figure 4d, e and extended Figure 3d, 5b and 6o (one experiment performed in 4 animals for Figure 4d, e).
Randomization	For in vivo and in vitro screening experiments, mice/cells from each treatment group were randomized for which treatment they received.
Blinding	Blinding was generally not done for these figures. However, all of our quantifications were performed in an automated fashion using software tools (e.g. QuPATH image analysis, Python CasTLE analysis, Varioskan plate reader). We did not select areas to image. We imaged and quantified the entire olfactory bulb or SVZ region. We have indicated that no blinding was done for these figures in the Methods section.

Reporting for specific materials, systems and methods

We require information from authors about some types of materials, experimental systems and methods used in many studies. Here, indicate whether each material, system or method listed is relevant to your study. If you are not sure if a list item applies to your research, read the appropriate section before selecting a response.

Materials & experimental systems

n/a	Involved in the study
☐	☒ Antibodies
☐	☒ Eukaryotic cell lines
☒	☐ Palaeontology and archaeology
☐	☒ Animals and other organisms
☒	☐ Clinical data
☒	☐ Dual use research of concern
☒	☐ Plants

Methods

n/a	Involved in the study
☒	☐ ChIP-seq
☐	☒ Flow cytometry
☒	☐ MRI-based neuroimaging

Antibodies

Antibodies used

Immunofluorescence: In vitro: GLUT4 (Abcam, 33780) 1:500, Ki67 (Invitrogen, 14-5698-082 clone SolA15) 1:500, STX4A (Santa Cruz Biotechnology, SC101301 clone QQ-17) 1:500. Alexa 488/594/647 conjugated antibodies, (Fisher Scientific, A21206, A21209, A31571) 1:500.
Immunofluorescence straining in brain sections in vivo: mCherry (Invitrogen, M11217 clone 16D7) 1:500, GFAP (Abcam, 53554) 1:500, GFP (Abcam, 13970) 1:500, GLUT4 (R&D Systems, MAB1262 clone 1F8) 1:500, Ki67 (Invitrogen, 14-5698-082 clone SolA15) 1:500, STX4A (Santa Cruz Biotechnology, sc-101301 clone QQ-17) 1:500, GFP (Abcam, 13970) 1:500, mouse IgG (Santa Cruz SC-3877, Lot: L1916) 1:500. Alexa 488/594/647 conjugated antibodies, (Fisher Scientific, A21202, A21206, A21209, A21447, A31571, A31573) 1:500, NeuN (Millipore, MAB377, clone A60) 1:500, S100a6 (Abcam, ab181975 clone EPR13084-69) 1:500, Tuj1 (Biolegend, 802001) 1:500, Olig2 (R&D Systems, AF2418) 1:100, Sox10 (Abcam, Ab180862 clone EPR4007-104) 1:100, Calretinin (Abcam, Ab244299) 1:500, Dcx (Cell Signalling Technology, 4604) 1:500.
Western blot: GLUT4 (Invitrogen, PA1-1065) 1:500. B-actin (Abcam ab6276) 1:40,000.
FACS: Ki67 (Ki67-APC (eBioscience, 17-5698-82) 1:300, GLUT4 (R&D Systems, MAB1262): diluted a 5:1 ratio with secondary anti-IgG AlexaFluor647, and the mix was added to live cells in culture at a dilution factor of 1:200.

Validation

The Ki67 antibody was validated by knockout in HeLa cells (by manufacturer) and in our manuscript by verifying that it only stained the nucleus of primary cultures of mouse activated NSCs (proliferative NSCs) and not quiescent NSCs (non-proliferative NSCs). The Dcx, Stx4a, S100a6, Olig2, Tuj1, Calretinin, and GLUT4 (Invitrogen, PA1-1065, used for western blot) antibodies were confirmed to stain the correct size band on western blot of rodent tissue/cells by the manufacturers. The mCherry/GFP antibodies were validated in mCherry-overexpressing human/mouse tissue and cell lines by western blot/immunofluorescence by the manufacturers. The NeuN, Tuj1, Olig2, Sox2, Calretinin, GLUT4(Abcam, 33780) and GLUT4(R&D Systems MAB1262, used for immunofluorescence and FACS) antibodies were validated by manufacturer by immunocytochemistry staining in rodent tissue, confirming correct morphological staining and regional specificity. The Ki67, Dcx and GFAP antibodies were also validated in vivo by examination of mouse coronal cryosections: Ki67 and DCX specifically marked cells in the SVZ neurogenic niche and along the rostral migratory stream (and no other regions), and the GFAP antibody displayed stereotypic cytoplasmic and projection GFAP staining present in both Ki67-positive (aNSCs) and Ki67- negative cells (qNSCs) but no Dcx+ cells (neuroblasts). Additionally, all three of these antibodies are widely cited in the literature. We also validated the GLUT4 antibodies that we used in immunocytochemistry (R&D Systems, MAB1262), FACS (R&D Systems, MAB1262) and western blot (Invitrogen, PA1-1065) by performing a CRISPR/Cas9-based knockout in this study.

Eukaryotic cell lines

Policy information about cell lines and Sex and Gender in Research

Cell line source(s)	293T cell line from ATCC (CRL-3216)
Authentication	Not authenticated
Mycoplasma contamination	Tested negative for mycoplasma
Commonly misidentified lines (See ICLAC register)	No commonly misidentified cell lines were used in the study

Animals and other research organisms

Policy information about studies involving animals; ARRIVE guidelines recommended for reporting animal research, and Sex and Gender in Research

Laboratory animals

Cas9-expressing mice (Cas9 mice) were obtained from Jax (https://www.jax.org/strain/024858). These mice (background C57BL/6N) constitutively express the Cas9 endonuclease and an EGFP reporter under the control of a CAG promoter knocked into the Rosa26 locus1. All screens in this study were performed with the Cas9 mice, including all NSC primary cultures and all in vivo work. We maintained a colony of Cas9 mice ranging in ages up to 28 months at the Stanford Comparative Medicine Building and the Neuroscience-ChemH building vivarium. As a negative control for the in vivo screens, male C57BL/6 mice obtained from the National Institute on Aging (NIA) Aged Rodent colony were used at 18-21 months old. NIA mice were habituated in the Stanford facility for at least 2 weeks prior to initiation of experiments. Mice were maintained under the care of the Veterinary Service Center at Stanford University under IACUC protocols 8661. Mice were housed in a 12 hour light/dark cycle, with ad libitum access to food/water, at 21o

	C and 50% humidity.
Wild animals	N/A
Reporting on sex	We have indicated the sex used in this study (both males and females were used).
Field-collected samples	N/A
Ethics oversight	At Stanford, all mice were housed in either the Comparative Medicine Pavilion or the Neuro Vivarium, and their care was monitored by the Veterinary Service Center at Stanford University under IACUC protocols 8661.

Note that full information on the approval of the study protocol must also be provided in the manuscript.

Plants

Seed stocks	N/A
Novel plant genotypes	N/A
Authentication	N/A

Flow Cytometry

Plots

Confirm that:

☒ The axis labels state the marker and fluorochrome used (e.g. CD4-FITC).

☒ The axis scales are clearly visible. Include numbers along axes only for bottom left plot of group (a 'group' is an analysis of identical markers).

☒ All plots are contour plots with outliers or pseudocolor plots.

☒ A numerical value for number of cells or percentage (with statistics) is provided.

Methodology

Sample preparation	For the genome-wide screen and for other qNSC reactivation experiments, we FACS-isolated proliferative cells (Ki67+) as follows. Cells were dissociated with Accutase (Stemcell Technologies, 07920) for 5 minutes, collected into conical tubes, and centrifuged at 300g for 5 minutes. Cells were resuspended in PBS at 5x10^7 cells in 1 mL (or 1x10^5 cell in 100 µL), and then 9 mL (or 900 µL) ice-cold 100% methanol was added and cells were agitated for 15 minutes at 4°C. Cells were then centrifuged at 500g for 5 minutes and resuspended for a wash in 3 mL PBS and centrifuged again at 500g for 5 minutes. Cells were then resuspended in 3.5 mL staining solution: Ki67-APC (eBioscience, 17-5698-82) 1:300 in PBS, 2% fetal bovine serum (FBS) (Gibco, 10099141) at 4°C. Samples were agitated for 30 minutes at room temperature in the dark, and then 10 mL PBS was added prior to centrifugation at 700g for 5 minutes. Samples were then resuspended (25 mL per 5x107 cells) in FACS buffer: PBS, 2% FBS, DAPI (Fisher Scientific, 62248, 1 mg/mL) 1:5000. Each sample was filtered with FACS-strainer cap tubes (Fisher, 08-771-23), just prior to FACS sorting. Cells were sorted on an Aria BD FACS Aria with a 100 µm nozzle at 13 psi and Flowjo (v10) software was used for data analysis.
Instrument	All cell sorting was performed using BD Aria II or BD PICI machine models housed in the Stanford Shared FACS Facility.
Software	Flowjo (v8) software was used for data analysis.
Cell population abundance	The %Ki67+ cells ranged from 2-40% depending on treatment and experimental setup.
Gating strategy	Gating was determined using fluorescent-minus-one controls for each color used in each FACS experiment to ensure that positive populations were solely associated with the antibody for that specific marker.

☒ Tick this box to confirm that a figure exemplifying the gating strategy is provided in the Supplementary Information.